ALGEBRAIC OVERTWISTED CONTACT STRUCTURES ON 3-SPHERE

by

Şeyma Karadereli

B.S., Mathematics, Boğaziçi University, 2017

Submitted to the Institute for Graduate Studies in
Science and Engineering in partial fulfillment of
the requirements for the degree of
Master of Science

Graduate Program in Mathematics

Boğaziçi University

2020

ACKNOWLEDGEMENTS

First and foremost, I would like to thank my advisor, Ferit Öztürk, for all his support, especially introducing me to this problem and explaining me every detail patiently. He was never tired to discuss mathematics with me whenever I visited his office. I appreciate his time and effort that made this thesis possible. No words can express my gratitude to him. I would also like to thank Çağrı Karakurt, especially for being so kind and supportive to me in my first year while I was feeling totally lost. I am grateful to know that he is there whenever I need advice or help. I would also like to thank Sergey Finashin, for his valuable remarks and advice on writing mathematics. It was great opportunity for me to have him in my thesis defense committee. I would like to acknowledge the Scientific and Technological Research Council of Turkey (TUBITAK) for funding this thesis by National Graduate Scholarship Programme (2210-E).

I am most grateful to my lovely family, especially to my dad for teaching me to fight for what I want and to my mom for being wise, supportive and loving in each period of my life. I am also grateful to know that my cousins, Beyza and Ahsen, are always here for me.

I owe much to Tuğba for being my second family. She witnessed this whole journey and is always there to listen and support me. Thank you for being so patient, especially during this pandemic. Thank you also to the other member of my second family, my dearest Şeyda, for her love and friendship. Moreover to Alperen, who is the secret hero of my math journey and to dear Mert for his valuable friendship. There are so many people to thank, but special thanks go to the small topology team, Fulya, Oğuz, and Turan for valuable discussions and time we spend together.

I dedicate this thesis to my cute babies Meryem, Meva, and Ömür. Your aunt loves you very much.

ABSTRACT

ALGEBRAIC OVERTWISTED CONTACT STRUCTURES ON 3-SPHERE

It is known that all of the complex analytic singularity links and the associated Milnor open books on the 3-sphere correspond to a single contact structure, which is the unique tight structure of the 3-sphere. The main question of this thesis is whether the overtwisted contact structures on the 3-sphere are real algebraic. We will define the notion of real algebraicity in the introduction of the thesis. We explicitly construct a family of real algebraic multilinks in the 3-sphere which are the bindings of planar Milnor open book decompositions supporting overtwisted contact structures. Furthermore, we prove that all the overtwisted contact structures with non-negative 3-dimensional invariants are obtained in this family.

ÖZET

3 BOYUTLU KÜRE ÜZERİNDEKİ CEBİRSEL AŞIRI DÖNEN KONTAK YAPILAR

Tüm kompleks analitik tekillik bağlarının ve 3 boyutlu küre üzerindeki ilgili tüm Milnor açık kitap ayrışımlarının tek bir kontak yapıya karşılık geldiği ve bu kontak yapının 3 boyutlu küre üzerindeki biricik sıkı kontak yapı olduğu bilinmektedir. Bu tezin temel sorusu; 3 boyutlu küre üzerindeki aşırı dönen kontak yapıların reel cebirsel olup olmadığıdır. Reel cebirsellik kavramını giriş bölümünde tanımlayacağız. Bu tezde, 3 boyutlu küre üzerinde, aşırı dönen kontak yapıları destekleyen düzlemsel Milnor açık kitap ayrışımların bağları olan bir reel cebirsel çoklu bağlar ailesi inşa ediyoruz. Ayrıca, 3 boyutlu küre üzerindeki, 3 boyutlu değişmezi negatif olmayan tüm aşırı dönen kontak yapıların bu aileyle elde edilebileceğini ispatlıyoruz.

TABLE OF CONTENTS

LIST OF FIGURES

LIST OF SYMBOLS

$A(\Gamma)$	The intersection matrix of the plumbed 4-manifold obtained by Γ
$c_1(\xi)$	The first Chern class of ξ
c^2	The square of the first Chern class
d_3	The 3-dimensional invariant
$\overline{f}$	Complex conjugate of the function f
$H_n(X, G)$	The n-th homology group of X with the coefficient group G
$H^n(X, G)$	The n-th cohomology group of X with the coefficient group G
$Hom(X, G)$	The set of homomorphisms from X to G
$lk(\cdot, \cdot)$	Linking number
L_f	The singularity link of the function f
$\mathbb{L}(\underline{m})$	The multilink with the homology class $\underline{m}$
Q_X	The intersection matrix of the manifold X
$rot(c)$	Rotation number of the curve c
$\mathrm{spin}^{\mathrm{c}}$	The $\mathrm{spin}^{\mathrm{c}}$ structure of a manifold
t_X	The twist map corresponding to the edge E
V_f	Germ of the analytic function f
λ	Longitude
μ	Meridian
$\sigma(X)$	The signature of the manifold X
ϕ	Monodromy map
$\chi(X)$	The Euler characteristic of X
Γ	Plumbing diagram
$\Sigma(\alpha_1, \cdots, \alpha_k)$	Seifert fibered manifold
$\Sigma_{g,r}$	The surface of genus g with r boundary component

1. INTRODUCTION

Contact structures on 3-manifolds come in two mutually exclusive types: overtwisted and tight. Y. Eliashberg proved that there is one-to-one correspondence between overtwisted contact structures up to contact isotopy and oriented 2-plane fields up to homotopy [1]. Combined with the fact that S^3 admits a unique tight contact structure, Eliashberg's result leads to a complete classification of the contact structures on S^3. The unique tight contact structure is induced by the standard embedding of the unit sphere in $\mathbb{C}^2$. The overtwisted contact structures on S^3 are countably infinitely many and they are determined uniquely by the 3-dimensional invariant d_3.

M. Gromov [2] and Eliashberg [3] showed that every Stein fillable contact structure is tight. Overtwisted contact structures are neither Stein fillable nor fillable in any other sense (see e.g. [4, Chapter 12] for the fillings of contact 3-manifolds). Additionally, there are also examples of tight structures which are not Stein fillable.

More generally, the singular complex analytic fillability of contact manifolds is discussed by C. Caubel, A. Némethi and P. Popescu-Pampu in [5]. The link manifold of an isolated singularity of a complex analytic surface V has a natural hypersurface distribution. A. N. Varchenko showed that this distribution is contact, which depends only on the analytic type of the complex surface singularity [6]. A *Milnor fillable* 3-manifold is a connected, closed, oriented contact 3-manifold which is contactomorphic to the link manifold of a complex analytic surface with an isolated singularity. Any such manifold admits a unique Milnor fillable contact structure up to contactomorphism [5, Theorem 1.2]. Moreover, if $f : (V, 0) \to (\mathbb{C}, 0)$ is a complex analytic germ with an isolated singularity at 0, the open book decomposition defined by the Milnor fibration of f (see e.g. [7]) is compatible with the Milnor fillable contact structure. (For the one-to-one correspondence between open book decompositions and contact structures in 3-dimension, one can see e.g [8] or [9].)

Every Milnor fillable contact structure is Stein fillable and hence is tight. A natural question one can ask is whether one can produce overtwisted contact structures in an analytical way. First recall that besides the existence of the Milnor fibration for isolated complex analytic singularities, Milnor also proved the existence of the Milnor fibration for the real analytic singularities under the condition that the Jacobian matrix of the function $h : \mathbb{R}^{n+k} \to \mathbb{R}^k$ has rank k on an open neighborhood of the origin, except the origin. [7]. We call this condition *Milnor condition*. Analytic constructions of overtwisted contact structures may depend on the Milnor fibration of the real analytic singularities. An immediate example is the overtwisted contact structure on S^3 with $\mathrm{d}_3 = \frac{1}{2}$. It is supported by the open book, with binding the negative Hopf link, which is given by the real algebraic map $h : \mathbb{R}^4 \to \mathbb{R}^2$, $h(x, y) = x\overline{y}$. Here we want to elaborate this type of constructions. Of course not every real analytic map satisfies the Milnor condition. Many studies have been conducted to find real algebraic maps admitting Milnor fibrations (see e.g. [10], [11]). Consider the holomorphic germs, $f, g : (\mathbb{C}^2, 0) \to (\mathbb{C}, 0)$ with isolated singularities. A. Pichon and J. Seade gave a wide family of link manifolds of real algebraic singularities of the form $f\overline{g}$ admitting Milnor fibrations [12]. (See also the sequence of articles [13], [14].)

We call the singularity links of complex algebraic plane curves in $\mathbb{C}^2$ *complex algebraic*. A link is *real algebraic* if it is the singularity link of an algebraic map $h : \mathbb{R}^4 \to \mathbb{R}^2$ that satisfies the Milnor condition. So every real algebraic link is a fibered link.

Which fibered links can be realized by real algebraic singularities is also discussed in many articles (e.g. [15] [16], [17]). One can ask that question even for multilinks instead of links. A multilink is a link together with integers, called multiplicities, on each of its link components. M. Ishikawa proved that if the multiplicities of a fibered multilink are all positive or all negative, the oriented multilink is the binding of an open book which is compatible with a tight contact structure [18]. He also proves that multilinks with opposite signed multiplicities are compatible with overtwisted contact structures. Thus, real algebraic fibered links can be obtained by such multilinks .

Since Milnor fillable contact structures are tight and there is a unique tight contact structure on S^3, it is compatible with an open book decomposition whose binding is a complex algebraic link. In this thesis, we explicitly construct real algebraic functions whose singularity links are fibered multilinks in S^3. Moreover, we show that these fibered multilinks are the bindings of open books supporting overtwisted contact structures on S^3, by computing the 3-dimensional invariants d_3 of the corresponding 2-plane fields. More precisely, we have:

Theorem 1.1. *Every overtwisted contact structure on S^3 with $\mathrm{d}_3 \geq 0$ is real algebraic. The associated real algebraic functions can be chosen of the form $f\overline{g}$ and the supporting open books to be planar.*

Here is the layout of the thesis text. In Chapter 2, we explain how to investigate the topology of link manifolds and singularity links by resolving the singular points. We present the Milnor condition for real analytic germs and state under which conditions the real analytic germs of the form $f\overline{g}$ satisfy the Milnor condition. In Chapter 3, we follow [19] to review multilinks in Seifert fibered manifolds. We explain the splicing operation for producing larger family of multilinks in homology 3-spheres and the cases when the splicing of two multilinks is possible. Afterwards, we explain how to use the combinatorial data of multilinks to detect fiberability and algebraicity of the multilinks. We describe the method discussed in [20] to calculate the d_3 invariant from the monodromy data and the pages of the compatible open book decomposition in Chapter 4. We give the constructive proof for Theorem 1.1 in Chapter 5. The detailed calculations concerning the intersection matrices which are necessary for the calculation of the d_3 invariant constitute the Appendix A.

2. RESOLUTION OF SINGULARITIES

For a thorough discussion of the material in this chapter, one can consult [21].

2.1. Links of Isolated Singularities

Consider the complex surface singularity $V = \{f_1 = \cdots = f_k = 0\} \subset \mathbb{C}^2$ for complex analytic polynomials $f_i : \mathbb{C}^2 \to \mathbb{C}$ with an isolated singular point $0 \in \mathbb{C}^2$. The intersection $V \cap S^3_\epsilon$ is a 3-manifold and is called a *link manifold*. Let $V_f \subset V$ be the germ of f. Since $0 \in V_f$ is an isolated singularity, V_f is complex co-dimension 1 submanifold of $\mathbb{C}^2$ and the intersection V_f with S^3_ϵ is transversal. Hence $V \cap S^3_\epsilon$ is a compact, smooth 1-manifold, embedded in the link manifold, and is called a *singularity link*. [22]

Since f is in the ring of convergent power series, it has a unique prime factorization i.e. $f = f_1^{n_1} \cdots f_k^{n_k}$ where each f_i is an irreducible complex polynomial. Thus, around the neighborhood of 0, the zero locus of f can be seen as $V_f = V_{f_1} \cup \cdots \cup V_{f_k}$ where each V_{f_i} is called a *branch* of V_f. For each irreducible component f_i, $V_{f_i} \cap S^3_\epsilon$ defines a component of the singularity link with a multiplicity. The *multiplicity* of a branch can be seen as the degree of f restricted to the branch at zero i.e. the intersection number of the parametrization of the branch and the curve V_f.

J. Milnor showed that V is locally homeomorphic to a cone on the singularity link whose vertex is the origin [7]. Hence, for the investigation of the topology of V around 0, it is sufficient to examine the topology of its link. For an extensive study about the topology of plane curve singularities, one can look up [23].

2.2. Resolutions of Singularities and Resolution Graphs

One of the main tools to study singularities is resolution. While we resolve singularities, we replace the singular points with larger sets (e.g. complex lines) to get a smooth manifold. Consider a singular curve $C \subset \mathbb{C}^2$ with an isolated singularity at 0. The space

$$\tilde{X} = \{(z_1, z_2, [a : b]) \in \mathbb{C}^2 \times \mathbb{C}P^1 | bz_1 = az_2\}$$

with $p : \tilde{X} \to \mathbb{C}^2$ a biholomorphic map away from the singular point, is called the *blow up* of $\mathbb{C}^2$ at 0. Observe that for any point $z = (z_1, z_2) \neq 0 \in \mathbb{C}^2$, $p^{-1}(z)$ consists of a single point, while $p^{-1}(0) = \{(0, 0, [a : b])\} \simeq \mathbb{C}P^1$, which will be denoted by E. Here, E is called the *exceptional divisor* and $\tilde{C} := \overline{p^{-1}(C - 0)}$ is called the *strict transform*. Note that $\tilde{X}$ is a smooth submanifold of $\mathbb{C}^2 \times \mathbb{C}P^1$, which can be covered by two charts

$$U_1 = \{(z_1, z_2, [a : b]) \in \tilde{X} | z_2 \neq 0, v_1 = z_2, u_1 = \frac{a}{b}\}$$

and

$$U_2 = \{(z_1, z_2, [a : b]) \in \tilde{X} | z_1 \neq 0, v_2 = z_1, u_2 = \frac{b}{a}\}$$

by pasting them by attaching $u_2 = \frac{1}{u_1}$ and $v_2 = u_1 v_1$. For any singular surface, we can always apply a finite number of blow ups to obtain a smooth complex surface $\tilde{X}$, which is called the *resolution of the singularity*.

Theorem 2.1. *Consider a complex surface singularity $(V, 0) \subset (\mathbb{C}^2, 0)$ with an isolated singularity at 0. There exist a smooth surface $\tilde{V}$ and a holomorphic map $p : \tilde{V} \to V$, which is a composition of a finite number of blow ups satisfying the condition:*

- *$E = p^{-1}(0)$ has smooth irreducible components $E_1, \cdots, E_t$ where $E_i \simeq \mathbb{C}P^1$ and they intersect each other transversally and pairwise disjointly.*

Here, $(\tilde{V}, p)$ is called a good resolution of $\mathbb{C}^2$.

We can correlate the combinatorial data of a good resolution with a weighted dual graph, which is called *dual resolution graph*. Each vertex symbolizes an irreducible component E_i of the exceptional divisor. For each E_i and E_j which intersect each other at a point, the vertices corresponding to them are joined by an edge. A dual resolution graph is decorated by the self intersection numbers of the exceptional divisors. When we acquire an exceptional divisor during the resolution process, its self intersection number is -1. As long as we continue blowing up a point of it, its self intersection number decreases by 1.

Let $f : (V, 0) \subset (\mathbb{C}^2, 0) \to (\mathbb{C}, 0)$ be a germ of an analytic function f. Let us define $T := \{f \circ p = 0\}$. It can be easily seen that $T = E \cup \tilde{C}$. Here, $\tilde{C}$ is the strict transform of $f^{-1}(0)$, which is a disjoint union of a finite number of irreducible smooth complex disks, each of which intersects E transversally at a smooth point. The components of the strict transform correspond to the preimage of the irreducible branches of V_f. The resolution graph for the germ of f is the resolution graph of $\tilde{V}$ decorated by arrowheads. Each arrowhead corresponds to the components of the strict transform and is attached to the vertices depending on the intersection of the strict transform with the exceptional divisors.

Example 2.1. Consider the holomorphic polynomial $f : \mathbb{C}^2 \to \mathbb{C}$ given by $f(x, y) = (x^2 + y^3)(x^3 + y^2)$, with two irreducible analytic factors $f_1 = x^2 + y^3$ and $f_2 = x^3 + y^2$. It can be easily seen that f has an isolated singularity at $(0, 0)$. Therefore, in order to understand the zero locus better, we will blow up the origin. On the first chart, we have the identification $\{x = st, y = t\}$ and on the second chart, we have $\{x = t', y = s't'\}$. Hence, $f(x, y) = 0$ gives $t^4(s^2 + t)(s^3t + 1) = 0$ on the first chart and $(t')^4(1 + (s')^3t')(t' + (s')^2) = 0$ on the second chart. We have $E_1 = \{t = 0\} = \{t' = 0\}$ with multiplicity $m_1 = 4$. In the first chart, f_2 is desingularized but not f_1, and in the second chart, the opposite. Hence, we will blow up the singular point of $f_1 = (s^2 + t)$ and $f_2 = (t' + (s')^2)$ in the corresponding charts.

On the first chart, we have singularity of $t^4(s^2+t)$ at the origin. After blowing up the origin with the charts $\{s = uv, t = v\}$ and $\{s = v', t = u'v'\}$, we have $v^5(u^2v+1) = 0$ and $(u')^4(v')^5(v'+u') = 0$. Here, $E_2 = \{v = 0\} = \{v' = 0\}$ with multiplicity $m_2 = 5$. In the first chart, f_1 is desingularized while in the second chart there is a triple transverse intersection of $\{f_1 = 0\}$, E_1 and E_2 at the origin. After one more blow up at the origin of the second chart by setting $\{u' = ab, v' = b\}$ and $\{u' = b', v' = a'b'\}$, the singularity resolves and we have $E_3 = \{b = 0\} = \{b' = 0\}$ with multiplicity $m_3 = 10$ which intersects E_2 and the component of the strict transform corresponding to $\{f_1 = 0\}$ at distinct points.

On the second chart, by blowing up twice in the same way, we get two exceptional divisors E_4, with multiplicity $m_4 = 5$, intersecting E_1 transversely and E_5, with multiplicity $m_5 = 10$, which intersects the second component of the strict transform and E_4 transversely in distinct points. In this example, the components of the strict transform have multiplicity 1. Moreover, the self intersection numbers corresponding to the exceptional curves are $e_1 = -5$,$e_2 = -2$, $e_3 = -1$, $e_4 = -2$, $e_5 = -1$. The dual resolution graph is given in Figure 2.1. The numbers in parentheses are multiplicities while the numbers on each vertex is the self intersection number of the corresponding exceptional divisor.

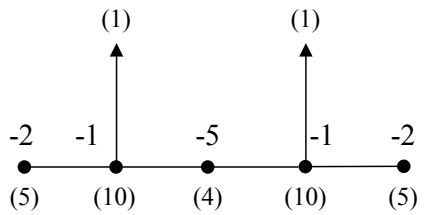

Figure 2.1. The resolution graph of Example 2.1

In [24], W.D. Neumann states that the dual resolution graph can be considered as a plumbing diagram (explained in Section 3.4) and one can construct a 4-manifold by applying plumbing operation according to the dual resolution graph. Consider a ball B^4_ϵ around 0. Since p is a biholomorphic map except 0, $p^{-1}(B^4_\epsilon)$ is also a 4-manifold,

which is a neighborhood of the exceptional divisors. The 4-manifold we obtained by the dual resolution graph is diffeomorphic to $p^{-1}(B^4_\epsilon)$. Moreover, the boundary of the plumbed manifold is diffeomorphic to the link manifold and $p^{-1}(V_f \cap S^3_\epsilon)$ is a link in the boundary of the plumbing manifold. The branch C_i of the strict transform corresponds to a link component on the boundary manifold and the multiplicity m_i of $p \circ f$ along the curve C_i gives the multiplicity of the corresponding link component. Therefore, the topology of the singularity link can be observed by the decorated resolution graph. In the next chapter, we will examine the singularity links as links in the boundary of the plumbing manifold.

2.3. Milnor Fibrations

Consider a holomorphic map $f : (\mathbb{C}^2, 0) \to (\mathbb{C}, 0)$ with a critical point at 0. We have the following Milnor Fibration Theorem [7, Chapter 4] which guarantees the existence of an open book decomposition in the case of isolated singularities.

Theorem 2.2. *Let ϵ be sufficiently small and $V_f = f^{-1}(0)$ be the zero set of f. Consider $L_f = V \cap S^3_\epsilon$. The map $\pi_f : (S^3_\epsilon - L_f) \to S^1$, $\pi_f(z) = \frac{f(z)}{|f(z)|}$, is a locally trivial fibration. If 0 is an isolated singularity of f, then L_f is fibered link which is the binding an open book decomposition of S^3 whose pages are fibers of the fibration, which are diffeomorphic to the Seifert surface of L.*

Later in the same book, Milnor proves that real analytic germs also give rise to such fibrations. We have the following theorem from [7, Chapter 11] (one can also see [13, Theorem 1.1]).

Theorem 2.3. *Let $f : (\mathbb{R}^4, 0) \to (\mathbb{R}^2, 0)$ be a real analytic germ whose Jacobian matrix has rank 2 on an open neighborhood of 0 i.e. f has an isolated singularity at 0. For ϵ sufficiently small, consider $L_f = V \cap S^3_\epsilon$ and let $N(L_f)$ be a tubular neighborhood of L_f. Then, there is a locally trivial fibration $\pi_f : (S^3_\epsilon - N(L_f)) \to S^1$ which is isomorphic to the fibration $f^{-1}(S^1) \cap D^4_\epsilon$.*

Here the fibration π_f can be chosen so that in the neighborhood of the link, it coheres with the map $\frac{f}{|f|}$. However, if 0 is not an isolated singularity then $\frac{f}{|f|}$ might not be a locally trivial fibration, hence does not define an open book decomposition. It is tough to find examples with isolated singularities in the real case. In the next section, we will examine some necessary and sufficient conditions for real analytic germs to have isolated singularities. One can look up [25] for a comprehensive investigation on Milnor fibrations and recent developments.

2.4. Real Algebraic Singularities of the Form $f\overline{g}$

In [13] and [12], Pichon and Seade examine real algebraic germs with isolated singularities of mixed functions of the form $f\overline{g}$ where f and g are holomorphic functions. They show the existence of the Milnor fibration in the link exterior and also investigate the geometry of the fibration near the singularity link. We have the following important results which enable us to consider the bindings of larger family of open book decompositions in S^3 as open book decompositions obtained by Milnor fibrations.

Theorem 2.4. [12, Theorem 2] *Let $f, g : (\mathbb{C}^2, 0) \to (\mathbb{C}, 0)$ be two holomorphic germs with no common branches. The following statements are equivalent:*

(i) The real analytic map $f\overline{g} : (\mathbb{R}^4, 0) \to (\mathbb{R}^2, 0)$ has an isolated singularity at 0.
(ii) $L_f - L_g$ is a fibered multilink. Here, $-L_g$ denotes L_g with reversed orientation.
(iii) For $p : \tilde{X} \to \mathbb{C}^2$ a good resolution of fg, we have $m_i^f \neq m_i^g$ for each rupture vertex i of its dual graph.

If any of these conditions hold, the Milnor fibration $\pi_{f\overline{g}} : S_\epsilon^3 - (L_f \cup L_g) \to S^1$ is a fibration of the multilink $L_f - L_g$ and isotopic to $\frac{f\overline{g}}{|f\overline{g}|}$ on the tubular neighborhood of the link, too. Hence it defines an open book decomposition of S^3.

We observe that $L_{f\overline{g}}$ as an unoriented link is $L_f \cup L_g$. We can obtain its plumbing diagram via the resolution graph of L_{fg} as in Section 2.2 by orienting link components corresponding to f positively and g negatively.

3. SEIFERT FIBERED MANIFOLDS

As we discussed in the previous chapter, the fibration on the link exterior, namely the Milnor fibration, constitutes an open book decomposition whose pages are Seifert surfaces of the singularity link. Therefore, to get information about the open book decompositions whose bindings are singularity links, we will examine topology of the algebraic links in S^3. Moreover, topological singularity link does not carry information about the multiplicities of the branches of the germs, whereas Milnor fibration is in the homotopy class determined by these multiplicities. That is why, we need the notion of multilinks, links with additional information, which is firstly introduced by Neumann and D. Eisenbud in [19]. By the Decomposition Theorem of W. H. Jaco, P. B. Shalen, K. Johansson and Thurston's Hyperbolization theorem, it is known that we can decompose every link in S^3 into torus links and hyperbolic links into pieces cutting along a tori. Any pieces we obtained after decomposing is either Seifert fibered or simple. In the case of algebraic links, it is known that each component has a Seifert fibered structure. Therefore, in order to study algebraic links, or more generally algebraic multilinks, it is convenient to understand the link's exterior and its decomposition.

In this chapter, we will define multilinks, in particular, Seifert multilinks. We will also give complete classification of them and a definition of Seifert fibered manifolds. To examine decompositions of the multilinks, we will define the splice operation. We will explain under which conditions this operation is valid and how we can read topological data from splice decompositions according to splice diagrams. We will explain how these results are related to plumbing manifolds, i.e. how these results are connected to the algebraic case. We mainly follow the arguments in [19].

3.1. Seifert Links and Multilinks

Definition 3.1. *A multilink* $\mathbb{L}(\underline{m}) = \mathbb{L}(m_1, \ldots, m_n) = (\Sigma, m_1 S_1 \cup \cdots \cup m_n S_n)$ *in an oriented homology 3-sphere* Σ *is a collection of smooth disjoint oriented simple closed*

curves together with integer multiplicities. We have the equality $m_iS_i = (-m_i)(-S_i)$ *where* $-S_i$ *is* S_i *with the opposite orientation.*

Equivalently, we can define a multilink as an oriented link L in Σ with a homology class $(m_1, \ldots, m_n) \in H_1(L) = \mathbb{Z}^n$. Note that, by Alexander Duality

$$H_1(L) \simeq H^1(\Sigma - L). \tag{3.1}$$

Also, by the Universal Coefficient Theorem, we know that

$$H^1(\Sigma - L) \simeq Hom(H_1(\Sigma - L), \mathbb{Z}). \tag{3.2}$$

Since $H_1(\Sigma - L)$ is generated by $\langle \mu_1, \ldots, \mu_n \rangle$ where μ_i is the standard oriented meridian of the component S_i, we can generate $H^1(\Sigma - L)$ with the set $\langle lk(\mu_1, \cdot), \ldots, lk(\mu_n, \cdot) \rangle$. Therefore, $\underline{m} = (m_1, \ldots, m_n)$ represents a cohomology class in the link complement given by,

$$\underline{m}(\gamma) = lk(L, \gamma) = \sum_{i=1}^{n} m_i \cdot lk(S_i, \gamma) \tag{3.3}$$

where $\underline{m}(\mu_j) = m_j$, $j = \{1, \cdots, n\}$.

We should note that an oriented link is a multilink with multiplicities ± 1, thus the notion of multilinks is a generalization of links.

Definition 3.2. *A Seifert surface for the multilink* $\mathbb{L}(\underline{m})$ *is an embedded oriented surface* $F \subset \Sigma - L$ *such that*

- *If* $m_i \neq 0$, $\overline{F} \cap N(S_i)$ *has* $|m_i|$ *leaves meeting along* S_i *and* F *is oriented in a way that* $F \cap \partial N(S_i) = m_iS_i$ *in* $H_1(N(S_i))$ *where* $N(S_i)$ *denotes the tubular neighborhood of the link's i-th component.*
- *If* $m_i = 0$, $\overline{F} \cap N(S_i)$ *comprises discs which are transverse to* S_i *and* F *is oriented*

in a way that the intersection number of S_i with each disc is the same and either $+1$ or -1.

Note that, $F \in H_2(\Sigma - L, \partial(\Sigma - L))$ and $H_2(\Sigma - L, \partial(\Sigma - L)) \simeq H^1(\Sigma - L)$ by Alexander Duality. On the other hand, since $F \cdot \mu_i = m_i = lk(L, \mu_i) = \underline{m}(\mu_i)$, we realize that the Seifert surface of a multilink is dual to the associated cohomology class of the multilink.

Seifert surfaces can be characterized as follows. Assume that $F \cap N(S_i) = a\mu_i + b\lambda_i$ and let $F_0 = F \cap (\Sigma - L)$. We have $\partial F_0 = a\mu_i + b\lambda_i + \sum_{j \neq i}^{n} m_j S_j$. Thus, we have $F_0 \cdot \mu_i = b$ and also by the previous paragraph $F_0 \cdot \mu_i = \underline{m}(\mu_i) = m_i$. Similarly $F_0 \cdot \lambda_i = \sum_{j \neq i}^{n} m_j lk(\lambda_i, S_j) + a = 0$ which implies $a = -\sum_{j \neq i}^{n} m_j lk(\lambda_i, S_j)$, we can denote $-\sum_{j \neq i}^{n} m_j lk(\lambda_i, S_j)$ as m_i'. Therefore, if we assume that $gcd(a, b) = d_i$ i.e. $d_i = (\frac{m_i}{p_i}) = (\frac{m_i'}{q_i})$ where $gcd(p_i, q_i) = 1$, we get $F \cap \partial N(S_i) = d_i S_i(p_i, q_i)$ where $S_i(p_i, q_i)$ is (p_i, q_i)-cable knot on S_i.

Because the fundamental group of the link exterior is abelian, we know that $Hom(H_1(\Sigma - L), \mathbb{Z}) \simeq Hom(\pi_1(\Sigma - L), \mathbb{Z})$ where the latter group is the set of homotopy classes of the maps from the link exterior to S^1. By the equation (3.2), this implies that the cohomology class $\underline{m}$ defines a homotopy class in $[\Sigma - L, S^1]$. We call a multilink *fibered* if there exists a locally trivial fibration map $\Sigma - L \to S^1$ in the homotopy class which corresponds to the multiplicities of the multilink whose fibers are minimal Seifert surface for the multilink.

Let Y be an oriented 3-manifold and B be an oriented surface. A *Seifert fibration* is a map $\psi : Y \to B$ such that all of its fibers are circles and in a disk neighborhood of any point x_i, preimage of the disk is homeomorphic to a solid torus where preimage of the center is core circle of the solid torus while any other point lifts to fibers of ψ that wrap α_i times in the longitudinal direction and $-\beta_i$ times in the meridianal direction around the core. Here, α_i and β_i only depends on x_i and they are relatively prime integers. If $\alpha_i = \pm 1$, the whole neighborhood is fibered trivially as $D^2 \times S^1$, the

core circle is called *nonsingular (generic) fiber* ψ. Otherwise, there are α_i fibers in the preimage of any point, in this case the core circle is called *singular (exceptional) fiber* of the map. When B is compact, the number of the singular fibers are finite [26]. Y is called *Seifert fibered manifold*.

Let $B_0 = S^2 - int((D^2)_1 \cup \cdots \cup (D^2)_k)$ be a 2-sphere with k punctures. Consider the trivial S^1-bundle $\Sigma_0 = B_0 \times S^1$ whose boundary consists of k tori $((S^1)_1 \times S^1) \cup \cdots \cup ((S^1)_k \times S^1)$. Let $R = B_0 \times \{1\}$ be a section of this bundle. Define $Q_i = R \cap ((S^1)_i \times S^1) = (S^1)_i \times \{1\}$ oriented as a component of $-\partial R$ and $H_i = \{1\} \times S^1 \subseteq {S^1}_i \times S^1$ which is a typical oriented fiber of the circle bundle on the i-th boundary component. Note that Q_i and H_i are generators of the first homology group of i-th boundary component. We paste a solid torus $T_i^2 = D^2 \times S^1$ onto the i-th boundary component $(S^1)_i \times S^1$ by gluing a meridian $\mu_i = S^1 \times \{1\}$ of the solid torus to the curve $\alpha_i Q_i + \beta_i H_i$ on $(S^1)_i \times S^1$ where α_i, β_i are relatively prime integers. For a chosen longitude $\lambda_i = \{1\} \times S^1$ for T_i^2, we have λ_i is homologous to $-\sigma_i Q_i + \delta_i H_i$ on ${S^1}_i \times S^1$ where $\sigma_i = \alpha_1 \ldots \widehat{\alpha_i} \ldots \alpha_k$ and $\delta_i = \sum_{j \neq i} \beta_j \alpha_1 \ldots \widehat{\alpha_i} \ldots \widehat{\alpha_j} \ldots \alpha_k$. The resulting manifold Σ is a homology 3-sphere if the coefficients α_i, β_i satisfies $\sum_{i=1}^{k} \beta_i \alpha_1 \ldots \widehat{\alpha_i} \ldots \alpha_k = 1$ [27]. We denote the manifold by $\Sigma(\alpha_1, \ldots, \alpha_k)$. When all α_i are nonzero, we can extend the circle bundle on Σ_0 to T_i's and have a Seifert fibration. The core circles S_i of the glued tori T_i are singular fibers of the fibration when $\alpha_i \neq \pm 1$ because of the way we glue the tori.

It can be easily seen that manifolds $\Sigma(\alpha_1, \ldots, \alpha_k)$ and $\Sigma(\alpha_1, \ldots, \alpha_k, 1)$ are homeomorphic. $\Sigma(\alpha_1, \alpha_2)$ is a basic example of a Seifert fibered 3-manifolds which is S^3. A *Seifert link* is defined to be an oriented link in $\Sigma(\alpha_1, \ldots, \alpha_k)$ which is the union of a finite number of singular and nonsingular fibers of the Seifert fibration. As an example, $(\Sigma(\alpha_1, \alpha_2, 1, \ldots, 1), S_1 \cup \cdots \cup S_n)$ consists of n copies of (α_1, α_2)-torus knot on S^3. Seifert links with multiplicities for each component are called *Seifert multilinks*.

3.2. Splice Decomposition, Splice Diagrams of Graph Links

In this section, we will define the operation called splicing. It is a generalization of the basic operations such as connected sum, disjoint sum and cabling. We will see that splicing can be used to construct new links from old ones and help us to define the fibrations of the new links with respect to the old ones. We will see that any multilink can be expressed as splicing of more elementary multilinks. For a short introduction to this subject, one can see [28].

Definition 3.3. *Let* $\mathbb{L}' = (\Sigma', m_0'S_0' \cup m_1'S_1' \cup \cdots \cup m_n'S_n')$ *and* $\mathbb{L}'' = (\Sigma'', m_0''S_0'' \cup m_1''S_1'' \cup \cdots \cup m_n''S_n'')$ *be two oriented multilinks. For a chosen pair of link components* ${S_0}'$ *and* S_0''*, consider their tubular neighborhoods with standard meridians and longitudes. Consider*

$$\Sigma = (\Sigma' - N(S_0')) \cup_h (\Sigma'' - N(S_0''))$$

where h *is the homeomorphism mapping meridians on the boundary of the tubular neighborhoods of the link components to longitudes and vice versa. The multilink*

$$\mathbb{L} = (\Sigma, m_1'S_1' \cup \cdots \cup m_n'S_n' \cup m_1''S_1'' \cup \cdots \cup m_n''S_n'')$$

is called the splice of $\mathbb{L}'$ *and* $\mathbb{L}''$ *along* ${S_0}'$ *and* S_0''*.* $\mathbb{L}'$ *and* $\mathbb{L}''$ *are called the splice components of* $\mathbb{L}$*.*

Σ is again a homology 3-sphere which can be seen easily by writing down Mayer Vietoris sequence.

In other respect, as we mentioned in the beginning of this chapter, splitting theorem of Jaco, Shalen and Johannson tells us that if L is a link in Σ, it is the result of a splicing operation along a torus, embedded in the link exterior, which is uniquely defined up to reversing the orientations of the link components that is spliced. The splice components which is obtained after desplicing the link is either a Seifert link or a simple link. Moreover, if the link is in S^3, the splice components are also in

S^3 [19, Proposition 2.1]. By definition, $\Sigma - L$ is the union of the link complements of splice components pasted along some torus. The multilink structure given by the cohomology class $\underline{m}$ determines the multilink structure of each splice component. In other words, $\underline{m} \in H^1(\Sigma - L) = H^1((\Sigma' - L')) \cup (\Sigma'' - L''))$ can be restricted to the classes $\underline{m}' \in H^1((\Sigma' - L')$ and $\underline{m}'' \in H^1((\Sigma'' - L'')$. Thus, splicing of links is possible if and only if these cohomology classes agree on the torus on which the splicing occurs. On this torus, we have

$$\begin{aligned} m'_0 &= \underline{m}'(\mu') = \underline{m}''(\lambda'') \\ m''_0 &= \underline{m}'(\lambda') = \underline{m}''(\mu'') \end{aligned} \tag{3.4}$$

Note that $\underline{m}''(\lambda'') = \sum_{i\neq 0}^{n} m''_i lk(\lambda'', S''_j)$ and $\underline{m}'(\lambda') = \sum_{i\neq 0}^{n} m'_i lk(\lambda', S'_j)$. Hence splicing is possible only when the multiplicity of splice components satisfies the above equalities. Observe that this equalities coincide with the characterization of Seifert surface given in the previous section. We can say that while splicing two links along a torus, we paste Seifert surfaces of splice components along the splicing torus.

We are interested in algebraic links, the special kind of multilinks that can be realized as link of plane curve singularities. As we have seen in the previous chapter, each branch of the germ of an analytic map carries a positive integer multiplicity. This multiplicity gives the multiplicity of the corresponding component of the singularity link. We call a multilink with splice components that are all Seifert links a *graph link*. Algebraic multilinks are known to have only Seifert fibered splice components that can be derived from Puiseux pairs [19, Appendix to Chapter 1], hence they are special family of graph links. All the graph links in S^3 are iterated torus links [19, Theorem 9.2].

Multilinks shall be represented by a special kind of diagrams that are called *splice diagrams*. Since graph links can be produced by splicing Seifert multilinks, we can represent all the graph links by splice diagrams which can be seen as a special combination of splice diagrams of splice components. Splice diagrams are practical for

many purposes such as computing linking numbers, defining whether a multilink is fibered, so on. They are explained in [19, Section 8] in depth.

Recall that we can express Seifert multilinks as $(\Sigma(\alpha_1, \ldots, \alpha_k), m_1 S_1 \cup \cdots \cup m_n S_n)$. It can be represented by a splice diagram given in Figure 3.1 where nodes correspond to Seifert manifold embedded in the link exterior, arrowhead vertices correspond to the tubular neighborhoods of link components (nonsingular fibers), whereas boundary vertices correspond to the tubular neighborhoods of some singular fibers of the Seifert manifold. Note that in [19, Chapter III], the node is also considered as a nonsingular fiber of the fibration of the corresponding Seifert manifold.

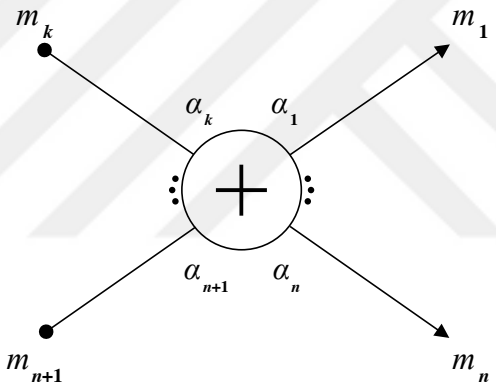

Figure 3.1. Splice diagram for a Seifert multilink

Splicing of two multilinks can be seen as connecting the splice diagrams of them along arrowheads corresponding to link components at which splicing occurs. Thus, splice diagrams of graph links can be easily obtained from splice diagrams of splice components. The splice diagram for a multilink is not unique, however up to some equivalence relations given in [19, Theorem 8.1], there is a unique minimal splice diagram.

Proposition 3.4. *Let v and w be two vertices in the splice diagram of a given multilink. Let $\sigma(v, w)$ be the simple path connecting vertices v and w. The linking number of the link components corresponding to v and w respectively is the product of all weights*

Figure 3.2. Splice diagram for a graph link

adjacent to $\sigma(v, w)$ *which are not on it.*

Example 3.1. Consider the Seifert multilink given in Figure 3.1. For $1 \leq i, j \leq k$,

$$lk(S_i, S_j) = \alpha_1 \dots \hat{\alpha}_i \dots \hat{\alpha}_j \dots \alpha_k.$$

Also, for any nonsingular fiber τ of Σ,

$$lk(\tau, S_i) = \alpha_1 \dots \hat{\alpha}_i \dots \alpha_k.$$

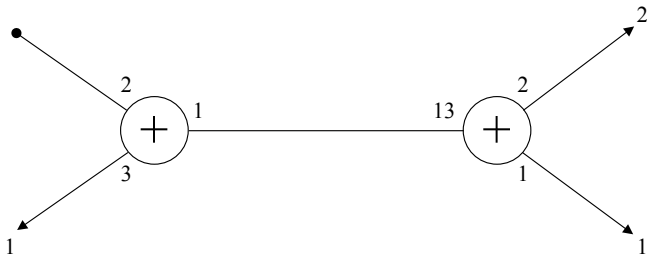

Figure 3.3. Splice diagram for the Example 3.2

Example 3.2. Consider the graph link given in Figure 3.3. It is the result of splicing of two Seifert links along the link components S_0', S_0'' corresponding to the weights $\alpha_0 = 1$, $\beta_0 = 13$ respectively. Observe that since $\underline{m}'(S_0') = m_1' lk(S_1', S_0') = 1 \cdot 2 = 2$ and $\underline{m}''(S_0'') = m_1'' lk(S_1'', S_0'') + m_2'' lk(S_2'', S_0'') = 1 \cdot 1 + 2 \cdot 2 = 5$, the multiplicities of the

splice components are $m_0' = 5$ and $m_0'' = 2$ by (3.4). The splice components of the link are given in Figure 3.4.

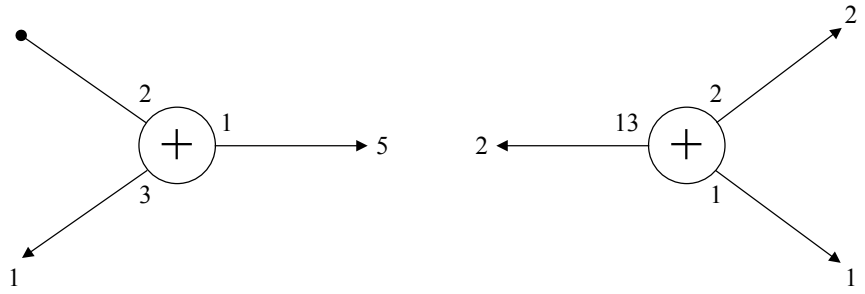

Figure 3.4. Splice components of the previous graph link

3.3. Fibered Condition of Graph Links and Monodromy

Recall that if a multilink is fibered, its fibers in the link exterior are Seifert surfaces bounded by the link itself. Since $\underline{m} \in [\Sigma - L, S^1]$, we have a circle bundle on the link exterior which the fibers of the fibration are transverse to. We say that any generic fiber of the manifold Σ intersects the pages of the fibration transversely in $|l|$ points which we will define below. In other words, the linking number of the multilink with any generic fiber (see Example 3.1) does not vanish. Moreover, since splicing operators paste the Seifert surfaces of splice components, for a multilink to be fibered, we need its splice components to be fibered, too. We summarize these results in the theorem below.

Theorem 3.5. *Let $\mathbb{L}(m) = (\Sigma, m_1 S_1 \cup \cdots \cup m_n S_n)$ be a Seifert multilink, it is fibered if and only if for any generic fiber τ of the manifold $\Sigma(\alpha_1, \ldots, \alpha_k)$, we have*

$$\underline{m}(\tau) = \sum_{i=0}^{n} m_i lk(\tau, S_i) \neq 0.$$

Furthermore, a multilink is fibered if and only if it is an irreducible link and each of its splice components is fibered.

We will denote $\underline{m}(\tau) = \sum_{i=0}^{n} m_i\sigma_i$ by l. Furthermore, the fibration $\pi : \Sigma - L \to S^1$ is unique up to homotopy and its fiber F has $d = gcd(m_1, \ldots, m_n)$ components which can be easily deduced from the exact homotopy sequence of the fibration [19, Theorem 11.3].

Moreover, when the multilink is fibered, $\Sigma - L$ is homeomorphic to the mapping torus of a diffeomorphism ϕ on F, i.e. it is homeomorphic to $F \times I/(0, x) \sim (1, \phi(x))$. We call the map ϕ the *monodromy* of the fibration. We have the following lemma summarizing useful results of this section.

Lemma 3.6. [19, Lemma 11.4] *Let $\mathbb{L}(m)$ be a Seifert fibered multilink, i.e. $l \neq 0$, given in Figure 3.1. Then, its fiber F is an $|l|$-fold cyclic branched cover of an n-punctured sphere and has Euler characteristic*

$$\chi(F) = |l| \cdot \left(k - 2 - \sum_{j=n+1}^{k} \frac{1}{\alpha_j} \right) \tag{3.5}$$

Furthermore, its monodromy ϕ is a generator of the group $\mathbb{Z}/|l|\mathbb{Z}$ of covering transformations. i.e. it is isotopic to a homeomorphism of order $|l|$. It can be seen as flows along the Seifert fibers of the link exterior on the interior of F, whereas it can be seen as flows along typical fibers H_i on each i-th boundary component.

Proof. The Seifert fibration ψ of $\Sigma(\alpha_1, \ldots, \alpha_k)$ can be seen as a S^1 action on Σ whose orbits are fibers of ψ. Consider this S^1 action on the link exterior $\Sigma - L$, the orbit space of this action $(\Sigma - L)/S^1$ is n-punctured sphere, call $\mathbb{S}_n$. Consider the Milnor fibration π on the link exterior with pages F. Let $z \in \Sigma - L$ and tz is an element of the orbit of z where $t \in S^1$. We have $\pi(tz) = t^l\pi(z)$ [19, p.90] which means only l of the points in the orbit map to the image of z. If the orbit of z is a nonsingular fiber of the Seifert fibration, it intersects F in l points. Nevertheless, if it is a singular fiber of the Seifert fibration, it wraps α_i times in the longitudinal direction, hence the orbit can be seen as $\mathbb{Z}/\alpha_i\mathbb{Z}$ and it intersects F in $\frac{l}{\alpha_i}$ points. By the map $\psi|_F$, we see that F is an $|l|$-fold branched cover of $\mathbb{S}_n$ with singular set consisting $k - n$ points with

branch indices $\alpha_{n+1}, \cdots, \alpha_k$. Hence, the monodromy $\phi : F \to F$ is a homeomorphism of order $|l|$ and can be seen as a flow along fibers. On the boundary of link exterior, the Seifert fibration has typical fibers H_i each of which is homologous to $\sigma_i\mu_i + \alpha_i\lambda_i$, we will explain the monodromy flow on the boundary in the next theorem. Moreover, By Riemann-Hurwitz Formula for branched covers,

$$\chi(F) = |l| \left(\chi(\mathbb{S}_n) - \sum_{i=n+1}^{k} \frac{\alpha_j - 1}{\alpha_j} \right).$$

Note that $\chi(\mathbb{S}_n) = 2 - n$.

We have already seen that the fiberability of a graph multilink depends on its splice components. The page of the graph multilink is also obtained by the pages F_i of the splice components pasted along a splicing torus. Hence, we can consider that the monodromy is pieced together from the monodromy maps of the splice components which are exactly $\phi|_{F_i}$ of finite order. If we take the tubular neighborhood of the separating tori in the link exterior, we see that the link exterior is the union of link exteriors of the splice components. Hence, we can see the Seifert fibered structure of the link exterior as the Seifert fibered structures of the link exterior of the splice components joined by toral annuli $T^2 \times I$. In each splice components, the monodromy is given by the flow along the corresponding Seifert fibers, whereas on the tubular neighborhood of the separating torus, it has two different flows in each end given by the Seifert fibration of each Seifert component. Monodromy acts like a twist map on the separating torus which measures the difference between two flows.

Theorem 3.7. [19, Theorem 13.1] *Let $F_i \cap F_j$ be the separating torus on which splicing of i-th and j-th splice components occurred and E be the edge of the splice diagram connecting these nodes as given in Figure 3.2. Let m_0' and m_0'' be the multiplicities of the splice components respectively and l_i and l_j be the orders of the monodromy map in each component. $F_i \cap F_j$ is the collection of $d_E = gcd(m_0', m_0'')$ annuli and in each of*

these annuli, the twist number is given by:

$$t_E = \frac{-d_E}{l_i l_j}(\alpha_0\beta_0 - \alpha_1 \dots \alpha_n\beta_1 \dots \beta_m). \tag{3.6}$$

For the boundary components, let $d_E = gcd(m_i, m')$ *where* m_i *is the multiplicity of the boundary component and* $m' = lk(S_i, \sum_{j\neq i}^{n} m_j S_j)$. *Let* α_i *be the weight of the corresponding component. We have*

$$t_E = \frac{-d_E}{m_i l}\alpha_i \tag{3.7}$$

Proof. Without lost of generality, we can assume that the graph multilink has two splice components with pages F_i and F_j. The graph multilink has the page $F = F_i \cup F_j$ and $F_i \cap F_j = T \cap F$ where T is the separating torus corresponding to tubular neighborhood of the link components which are spliced. Hence $T \cap F$ is the boundary component of both F_i and F_j. As we discussed the behavior of the page around the boundaries in Section 3.1 and 3.4, we have $F \cap T = m_0'\lambda' - m_0''\mu'$. hence $F \cap T$ has d_E components each of which is homologous to

$$\frac{m_0\prime}{d_E}\lambda' - \frac{m_0''}{d_E}\mu'. \tag{3.8}$$

On the one end of tubular neighborhood of the separating torus, we have the Seifert fibration corresponding to the first splice component. On the boundary that splicing occurred, it has fibers $H_i = \alpha_0\lambda' + \alpha_1 \cdots \alpha_n\mu'$. Similarly on the other end of the tubular neighborhood of the separating torus, the fibers of Seifert fibration on the boundary is given by $H_j = \beta_1 \cdots \beta_m\lambda' + \beta_0\mu'$. The monodromy flow runs parallel to the former at speed $1/l_i$, while to the latter at speed $1/l_j$. After some modifications as in [19, p.107,108]. We see that the difference of these two flows is a flow of speed (3.6) around (3.8). Similarly, on the boundary of the page, we have the flow (3.7).

3.4. From Plumbing Diagrams to Splice Diagrams

Recall from Chapter 2 that the resolution graphs of the links of singularities can be seen as plumbing diagram of the link in the corresponding the plumbing manifold. Thus, homology spheres of the fibered multilinks can be described by plumbing. In this section, we will give an algorithm to detect corresponding splice diagrams to links in the plumbing manifolds. In [19, Chapter 5], one can find more information about plumbing manifolds, algorithms to calculate the determinant of intersection form for plumbing manifold and how to obtain plumbing diagrams from splice diagrams.

We define a *plumbing tree*, denoted by Γ_0, to be a connected graph with no cycles which consists of vertices with an integer weight e_i and edges connecting some of the vertices. Given a plumbing tree Γ_0, one can construct an oriented 4-manifold obtained by plumbing disc bundles according to Γ_0 as constructed in [19]. The boundary of the 4-manifold is a plumbed 3-manifold which we will denote by $M(\Gamma_0)$. We define *plumbing diagrams*, denoted by Γ, to be plumbing trees with extra vertices which have one incident edge that shown by an arrow. Such a diagram represents a link $L(\Gamma)$ in the 3-manifold $M(\Gamma_0)$. If $M(\Gamma_0)$ is a homology sphere, then $L(\Gamma)$ is a graph link. Moreover, it is a Seifert fibered homology sphere and each vertex with more than 2 incident edges corresponds to a Seifert pieces of the manifold and arrows correspond to components of the given link. Let $\mathbf{V}(i)$, $\mathbf{A}(i)$, $\mathbf{N}(i)$ be the set of vertices, arrowhead vertices and non arrowhead vertices of Γ which are adjacent to i, respectively. Consider the intersection matrix $A(\Gamma) = (A_{ij})_{i,j\in\mathbf{N}}$ of the plumbed 4-manifold given below:

$$A_{ij} = \begin{cases} e_i, & i = j \\ 1, & j \in \mathbf{N}(i) \\ 0, & otherwise \end{cases}$$

$M(\Gamma_0)$ is a homology sphere if and only if $\det(A(\Gamma)) = \pm 1$. Note that an easy algorithm to calculate the determinant of a plumbing diagram can be found in [19, Section 21]. Moreover, if the plumbing tree Γ_0 can be reduced to a trivial graph by blowing down

(-1) vertices, then $M(\Gamma_0)$ is S^3. When $M(\Gamma_0)$ is a homology sphere, a cohomology class $\underline{m} \in H^1(M(\Gamma))$ gives a multilink structure on $(M(\Gamma), L(\Gamma))$, we can denote it as $\Gamma(m)$. All the previous results about link components also hold for $L(\Gamma)$. Up to replacing $\Gamma(-m)$ by $\Gamma(m)$, any graph multilink can be represented as unique plumbing diagram which has weight $e_i \leq -2$ for any vertex i which is neither an arrowhead nor a node. Recall from Chapter 2, the branches of $V = f^{-1}(0)$ have multiplicities that can be read from blow up steps, thus the singularity link is a multilink in S^3_ϵ. The decorated dual resolution graph is indeed the plumbing diagram for the singularity link and we can deduce the corresponding splice diagram using plumbing diagram to find out important results about the fibration whose binding is the multilink. The splice diagram for Γ for a multilink can be constructed as described below.

(i) Make $\det(-A(\Gamma)) = \pm 1$ by single $(+1)$ blow up on some chain of Γ. Since our link of singularities is in S^3, we can have a minimal plumbing diagram with determinant ± 1.

(ii) Replace each maximal chain in Γ by a single edge where all the nodes are weighted as 1.

(iii) Let Γ_i be the subgraph of Γ cut off by a corresponding edge of Γ. The weight at the end of that edge is given by $\det(-A(\Gamma_i))$. If Γ_i is a single arrowhead, $\det(-A(\Gamma_i)) = 1$.

(iv) Multiplicities are equal to the corresponding multiplicity in Γ.

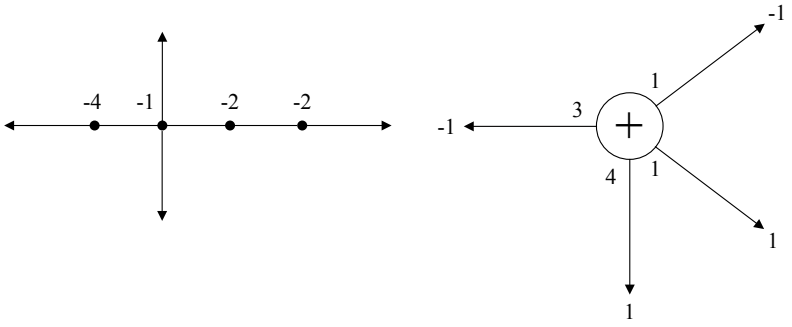

Figure 3.5. A Plumbing diagram on the left and the corresponding splice diagram on the right

As an example, consider the real analytic function $f\bar{g} = x\bar{y}(x^4 + \xi y^3)\overline{(x^4 + \xi^2 y^3)}$. Its dual resolution graph can be obtained as in Section 2.2 by resolving fg and orienting the branches corresponding to $\overline{g}$ negatively. It can be easily seen that $\det(-A(\Gamma)) = \pm 1$ and we have 4 maximal chains that we have to replace with single edges. The maximal chain on the left gives a subgraph with determinant 4, whereas the maximal chain on the right gives a subgraph with determinant 3. The other arrowheads are weighted as 1. The plumbing graph and the corresponding splice diagram are given in Figure 3.5.

3.5. Criteria for Algebraicity of Multilinks

After the discussion about fibered multilinks, the natural question that comes to mind is when a fibered multilink can be realized by singularities. As in Chapter 2, when we have an isolated singularity of a holomorphic function, the corresponding Milnor fibration defines an open book structure of S^3 whose binding is isotopic to the singularity link. All the complex algebraic links in S^3 are graph multilinks and the corresponding splice diagram of the multilink can be deduced from Puiseux pairs given in [19, Appendix 1]. However, not all the graph multilinks in S^3 are complex algebraic. The next theorem tells when a graph multilink is complex algebraic.

Theorem 3.8. [19, Theorem 9.4] *A multilink with positive weights and multiplicities which is represented by the splice diagram given in Figure 3.2 is an algebraic graph link if and only if its diagram satisfies* $\alpha_0\beta_0 > \alpha_1 \dots \alpha_n\beta_1 \dots \beta_m$.

The case of real analytic germs is more complicated. S. Akbulut and H. King showed in [29] that every knot (hence link) in S^3 is weakly real algebraic i.e it is the zero locus of an algebraic map $f : \mathbb{R}^4 \to \mathbb{R}^2$ with an critical point. However, even though the zero locus has a critical point, f might not have an isolated singularity at that point. Therefore, given any fibered multilink in S^3, we might not be able to find a real analytic map such that the Milnor fibration of the germ defines the open book decomposition of the fibered multilink. It is hard to construct examples of real analytic germs with an isolated singularity and it has been long studied in many articles.

Theorem 3.9. [12, Theorem 3] *If L_1 and L_2 are two multilinks in S^3 with positive multiplicities such that $L_1 \cup -(L_2)$, L_1 and L_2 are fibered multilinks, then there exist two holomorphic germs $f, g : (\mathbb{C}^2, 0) \to (\mathbb{C}, 0)$ without common branches so that L_1 and L_2 are isotopic to the link of singularities of f and g and $L_1 \cup -(L_2)$ is the multilink associated to the real analytic germ $f\overline{g} : (\mathbb{R}^4, 0) \to (\mathbb{R}^2, 0)$ given by $\frac{f\overline{g}}{|f\overline{g}|}$.*

Since we can check whether a multilink is fibered or not as in Section 3.3, we can obtain infinite family of real algebraic multilinks obtained from the holomorphic cases. The fiberability of $L_f \cup -(L_g)$ can also be checked using the dual resolution graph as it is discussed in [12] and Theorem 2.4.

4. INVARIANTS OF 4-MANIFOLDS

In this chapter, we will discuss a method to calculate the 3-dimensional invariants of the contact structures on S^3 regarding the compatible open book decompositions.

4.1. The 3-Dimensional Invariant of 2-Plane Fields

Consider the space of all 2-plane distributions on a 3-manifold Y, of which the set of contact structures is a subspace. Eliashberg proved that any contact structures which belong to the same component of this subspace are homotopic and each component contains an overtwisted contact structure [1]. However, we cannot conclude that homotopic contact structures are unique up to contact isotopy. As an example, we can consider the standard tight contact structure and the standard overtwisted contact structure on S^3, which are in the same homotopy class but not isotopic. We have the following results by Eliashberg which let us classify the contact structures on S^3 up to isotopy by focusing on the homotopy classes of 2-plane distributions.

Theorem 4.1. [1, Theorem 1.6.1] *Two overtwisted contact structures on a closed, oriented 3-manifold are isotopic if and only if they are homotopic as 2-plane distributions.*

Theorem 4.2. [30, Theorem 2.1.1] *Any tight contact structures on S^3 is isotopic to the standard contact structure.*

V. G. Turaev worked on construction of invariants for 2-plane fields [31]. Consider the space of vector fields of unit length in a 3-manifold Y. Two vector fields which do not vanish anywhere are said to be homologous if they are homotopic outside of a 3-ball in Y. An *Euler structure* is defined to be an equivalence class of homologous vector fields on Y. This structure is also called spin^c structure in the literature. Later on, R. E. Gompf worked on spin^c structures which make the classification of the contact structures easier [32]. Since there is a bijection between the space of oriented 2-plane fields and the space of vector fields of unit length, mapping each oriented 2-plane

field to its oriented normal vector field, we can consider a spin^c structure as induced by an oriented 2-plane field ξ which only depends on the homotopy type of ξ. Let $c_1(\xi) \in H^2(Y;\mathbb{Z})$ denotes the first Chern class of ξ. When $H^2(Y;\mathbb{Z})$ has no 2-torsion, if $[\xi_1]$ and $[\xi_2]$ are 2-plane fields satisfying $c_1(\xi_1) = c_1(\xi_2)$, they induce the same spin^c structure. Since $H^2(S^3;\mathbb{Z})$ is trivial, $c_1(\xi) = 0$ for any ξ and S^3 has a unique spin^c structure. Gompf also states that even if two 2-plane fields induce the same spin^c structure, they might not be homotopic. Their homotopy types are determined by d_3 invariant of ξ, which is defined by Gompf as

$$\mathrm{d}_3(\xi) = \frac{1}{4}(c_1^2(X,J) - 3\sigma(X) - 2\chi(X))$$

where (X, J) is a compact almost complex 4-manifold with boundary S^3 so that the oriented complex tangencies along S^3 are homotopic to ξ, $\sigma(X)$ and $\chi(X)$ are the signature and the Euler characteristic of X, respectively.

Let (Y, ξ) be a contact structure compatible with an open book decomposition with monodromy ϕ which is given by a product of Dehn twists around homologically nontrivial curves $\gamma_1, \cdots, \gamma_n$ on the page $\Sigma_{g,r}$ of genus g with r boundary components. We will give a method to calculate the d_3 invariant of the 2-plane field ξ by means of the corresponding open book decomposition. We will briefly follow arguments from [20]. It is a well known fact that for every 3-manifold Y with an open book decomposition, there exists a 4-manifold X with an achiral Lefschetz fibration such that $\partial X = Y$ and the achiral Lefschetz fibration agree with the open book decomposition on the boundary [33]. Moreover, we have the following fact proved by F. Ding and H. Geiges.

Theorem 4.3. [34] *Any closed orientable contact 3-manifold (Y, ξ) is the result of a sequence of ± 1 contact surgeries along a Legendrian link in (S^3, ξ_{std}).*

Recall that a link (Y, ξ), all of whose tangent vectors lie in ξ, is called a *Legendrian link*. The homotopy invariants of the contact structure can be gathered from the surgery description of a contact 3-manifold [35]. A contact surgery with an integer

surgery coefficient on a Legendrian knot can be seen as adding vanishing cycles to the achiral Lefschetz fibration of the 4-manifold, which bounds the contact 3-manifold [4].

Consider a 4-ball union $(2g + r - 1)$ 1-handles, $X_0 = \natural_{2g+r-1} S^1 \times D^3$ given in Figure 4.1. From the Kirby diagram of the manifold, it can be easily seen that it admits an honest Lefschetz fibration with no critical points, therefore it is diffeomorphic to the Stein manifold $D^2 \times \Sigma_{g,r}$. (See [36, Section 8.2] for the relations between Kirby diagrams and Lefschetz fibrations.) The fibration is a trivial bundle and its monodromy is trivial. Consequently, on the boundary, it admits an open book decomposition with the trivial monodromy and pages $\Sigma_{g,r}$, which is compatible with the standard contact structure on Y.

We can construct (Y, ξ) via a sequence of contact ± 1 surgeries on a Legendrian link on the boundary manifold as stated in Theorem 4.3. Consider γ_i's $\in Y$ as embedded in different fibers of the open book. It is known that every link is isotopic to a Legendrian link [36], thus we can consider these curves as a Legendrian link in Y and apply (± 1)-surgery on each component of this Legendrian link to construct ξ, depending on whether the Dehn twist around the link component is negative or positive. Each (-1)-surgery adds a vanishing cycle to the Lefschetz fibration and results an honest Lefschetz fibration which admits an almost complex structure. However, applying $(+1)$-surgeries gives an achiral Lefschetz fibration which does not have an almost complex structure. The resulting achiral Lefschetz fibration admits the open book decomposition on the boundary, Y, which is compatible with the desired contact structure ξ. In [35], it is shown that if X_1 is the handlebody decomposition of the 4-manifold admitting the Lefschetz fibration constructed via q $(+1)$-surgeries, ∂X_1 is the boundary of $X = X_1 \# q\mathbb{C}P^2$ and is a contact manifold with desired contact structure. Hence we can obtain every contact structure (S^3, ξ) by means of the monodromy data of the compatible open book decomposition.

Finally, we have following statement from [20] which is a generalization of the similar statement in [35].

Theorem 4.4. *Consider the 4-manifold X with $\partial X = (S^3, \xi)$, as we discussed above. Let $\sigma(X)$ be the signature, $\chi(X)$ be the Euler characteristic of X and q be the number of $(+1)$ surgeries we performed. The Chern class $c \in H^2(X;\mathbb{Z})$ is Poincaré dual to*

$$\sum_{i=1}^{n} rot(\gamma_i) C_i$$

where C_i's are the cocores of the 2 handles attached along γ_i. The 3-dimensional invariant d_3 is well-defined and is a rational number. Its formula is given by

$$\mathrm{d}_3(\xi) = \frac{1}{4}(c^2 - 3\sigma(X) - 2\chi(X)) + q \tag{4.1}$$

For any 2-plane field ξ on S^3, the corresponding 3-dimensional invariant is an element of $\mathbb{Z} - \frac{1}{2}$ [35, Remark 2.6]. In the next sections, we will explain how to calculate each of the terms of the formula.

4.2. 4-Manifold Construction via Pages and the Monodromy Data of Open Books

The 4-manifold, which is given as D^4 union $(2g+r-1)$, 1-handles is diffeomorphic to $D^2 \times \Sigma_{g,r}$ as we discussed in the previous section. After attaching four 2-handles, the corresponding manifold has a Kirby diagram given Figure 4.1, which is shown before in [20]. The dashed line presents the boundary, whereas the dotted lines present generators of the second homology of the page. Observe that the curves in the diagram represent the 2-handles attached along the Legendrian realizations of γ_i's with framing (± 1), depending on their positions with respect to each other in the pages.Moreover, note that the trivialization of the tangent bundle of the pages are observed in the Kirby diagram with the orientation induced from $\mathbb{R}^2$ [36]. Since the rotation number is computed as the winding number of the curves with respect to a standard trivialization of the tangent bundle of $\Sigma_{g,r}$, in order to calculate rotation numbers of these curves, we can compute the winding numbers of their images that are drawn in the diagram [37].

In the Figure 4.1, the red, purple and orange curves have rotation number zero whereas the blue curve has 1.

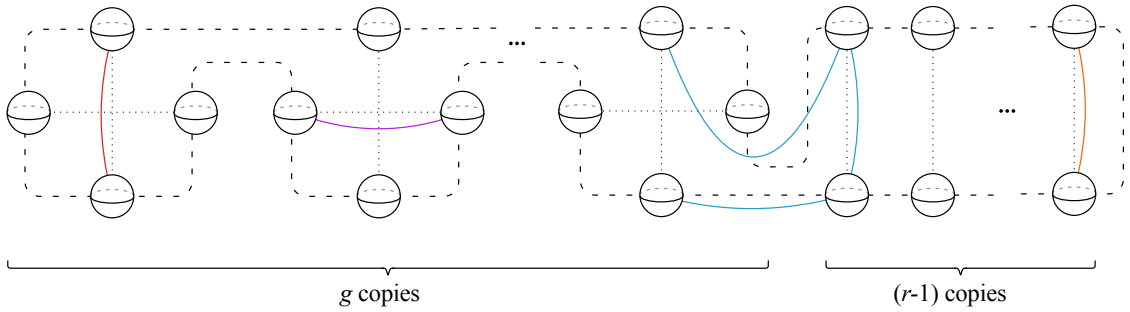

Figure 4.1. $D^4 \cup \{(2g + r - 1)$ 1-handles $\} \cup \{$four 2-handles$\}$

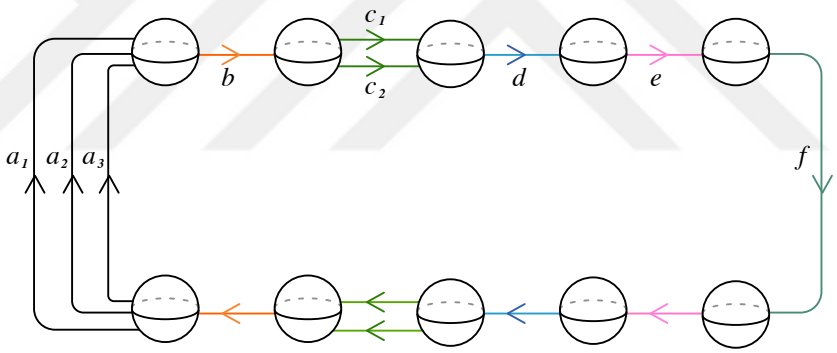

Figure 4.2. Kirby diagram for 4-manifold whose boundary admits an open book with planar pages

In this thesis, we focus on the open book decompositions which have planar pages with n boundary components and trivial monodromy in the interior of the pages. Therefore, the monodromy is represented as curves which are parallel to the boundary components. As an example, the Kirby diagram of a 4-manifold, which admits an open book decomposition with planar pages of 6 boundary components, is given in Figure 4.2.

4.3. Classical Invariants of 4-Manifolds

The *intersection form* for a 4-manifold is a symmetric 2-form

$$\mathbb{Q}_X : H_2(X;\mathbb{Z}) \times H_2(X;\mathbb{Z}) \to \mathbb{Z}$$

such that for any $\alpha, \beta \in H_2(X;Z)$, it is geometrically defined as the intersection number of the embedded surfaces corresponding to α, β. An intersection form can be expressed as a square symmetric matrix Q_X. The signature of this matrix gives the signature of the manifold X.

Since k-handles correspond to k-cells in the cell decomposition of the manifold, they form a basis for $C_k(X;\mathbb{Z})$. Thus, $H_2(X;\mathbb{Z})$ can be generated by using 2-handles by means of the boundary map which can be read from the Kirby diagram. In Figure 4.2, $H_2(X;\mathbb{Z})$ has the basis $\{a_1-a_2, a_2-a_3, c_1-c_2, a+b+c+d+e-f\}$. Since $\operatorname{rank} H_0 = 1$ and $\operatorname{rank} H_1 = 0$, the Euler characteristic of X is given by $\chi(X) = \operatorname{rank} H_0 + \operatorname{rank} H_2$.

The corresponding embedded surfaces for these basis elements are discussed in [35] as follows. Generators of the second homology group can be seen as a link in the boundary of D^4 due to the Kirby diagram of X [36]. We consider the Seifert surfaces bounded by the link components and push the interior of these Seifert surfaces into D^4. By adding the core of the 2-handles, we obtain closed embedded surfaces whose fundamental class also generate $H_2(X;\mathbb{Z})$. Thus, the intersection matrix can be considered as the linking matrix of the link.

Chern classes are defined to be the characteristic classes for complex vector bundles. Once we have a complex vector bundle over a manifold, it naturally induces a complex structure, which is called *almost complex structure*. Hence, we can specify Chern classes via the almost complex structures. In such cases, Chern classes are denoted by $c_i(X,J) \in H^2(X;\mathbb{Z})$. By [32], it is known that $c_1(X,J) \in H^2(X;\mathbb{Z})$ is defined by the surgery curve as its rotation number. Moreover, by Poincaré duality, its dual

to $\sum_{i=1}^{n} rot(\gamma_i)C_i$ as we mentioned before. When we calculate $c_1(X, J)$ as above in the basis we have chosen for $H_2(X)$, say it is a vector v^T, we can calculate square of it by

$$c^2(X) = v^t Q_x^{-1} v.$$

5. CONSTRUCTION OF CONTACT STRUCTURES ON 3-SPHERE VIA FIBERED MULTILINKS

Ishikawa states that a fibered graph multilink is compatible with a tight contact structure if and only if all of its multiplicities are either positive or negative [18]. For the multilinks with both positive and negative multiplicities, he constructs overtwisted disks around negative fibers to show that the corresponding contact structures are overtwisted. On S^3, we stated that all algebraic graph multilinks with positive (or negative) multiplicities are isotopic to the links of holomorphic germs with isolated singularities. On the other hand, by Section 3.5, we have concluded that we can produce an infinite family of real algebraic multilinks of the form $f\overline{g}$ via holomorphic germs. In other words, we can construct an infinite family of overtwisted contact structures on S^3.

In [38], J. B. Etnyre showed that all overtwisted contact structures on compact 3-manifolds are supported by planar open books. The question that comes to mind is whether all these planar open books are chosen to have algebraic bindings. To answer this question for the case of S^3, we will consider the family of fibered multilinks with planar Seifert surfaces. We construct special families of some real analytic maps that determine fibered links in S^3 which have trivial geometric monodromy. Recall from Chapter 3 that, since the monodromy map is of order $|l|$, for multilinks with $|l| = 1$, a page of the corresponding fibration is an $|l|$-fold branched covering of a punctured sphere, i.e. it is planar. Multilinks with $|l| = 1$ are given in Figure 5.1 ([19, p.123]). Note that these are all the possible Seifert multilinks with trivial monodromy. Firstly, we will show which real analytic maps have these links as singularity links. We will calculate the d_3 invariants of the corresponding contact structures to show that all overtwisted contact structures on S^3 are supported by real algebraic planar open books.

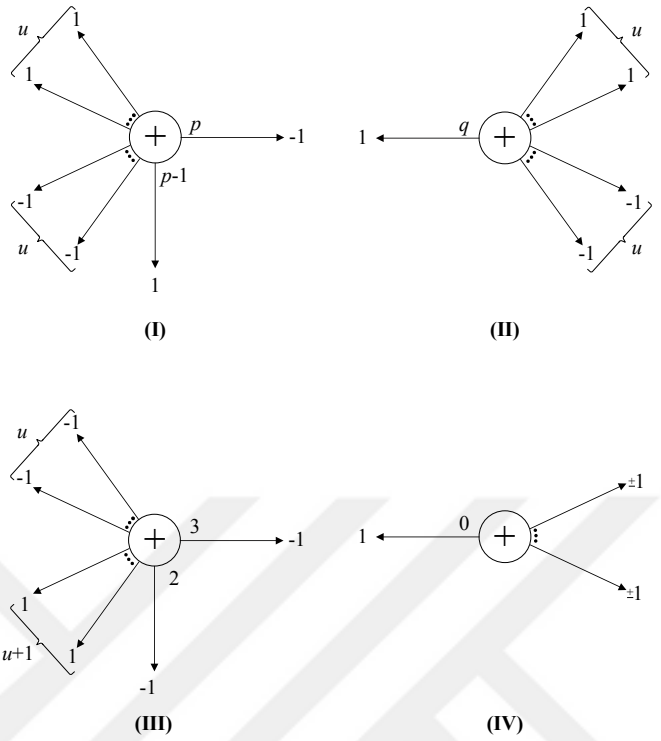

Figure 5.1. Families of multilinks in 3-sphere with trivial monodromy

Example 5.1. For the first example of an algebraic link with trivial monodromy, let $p \in \mathbb{Z}^+$ and α is a primitive (2u+1)-st root of unity i.e. $\alpha^{2u+1} = 1$. We consider two holomorphic functions:

$$f(x,y) = y\prod_{i=1}^{u}(x^p + \alpha^i y^{p-1}) \text{ and } g(x,y) = x\prod_{j=u+1}^{2u}(x^p + \alpha^j y^{p-1}).$$

Consider the real analytic function $f\overline{g}$. After a finite sequence of blow-ups, it can be easily seen that this function satisfies (iii) in Theorem 2.4 and is fibered. It has the dual graph given in Figure 5.2

This singularity link is isotopic to the plumbing link in S^3 given by the same diagram. In order to find the corresponding splice diagram, we will follow the algorithm

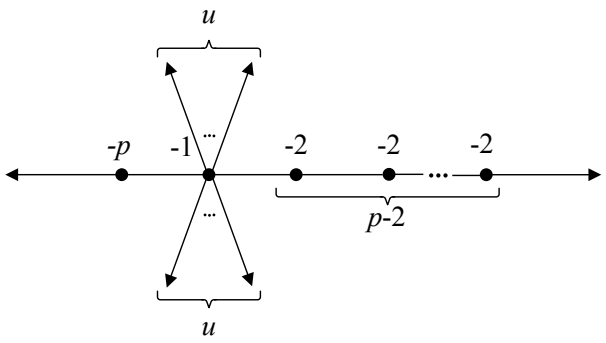

Figure 5.2. Plumbing diagram for (I)

we mentioned in Section 3.4. By simple matrix calculations, it can be easily checked that the determinant of the corresponding matrix is 1 whereas the left subgraph has determinant p and the right subgraph has determinant $(p-1)$. We conclude that the corresponding splice diagram is (I) in Figure 5.1.

Here, $l = -(p-1)+p-u\cdot p\cdot(p-1)+u\cdot p\cdot(p-1) = 1$. Hence, (I) is a fibered link with trivial geometric monodromy. Since all the multiplicities are either 1 or -1, the pages are connected and have only one leaf in the tubular neighborhood of each link component. Moreover, they are "1-fold" covering of $(2u+2)$-punctured S^2. Hence, the pages are $(2u+2)$-punctured spheres; denoted by, $\Sigma_{0,2u+2}$. (See Figure 5.3.)

Since $l = 1$, the monodromy is trivial in the interior of pages. However, the monodromy flow has nontrivial contribution on the boundary of the pages. By Theorem 3.7, the twist on each boundary components is given by $t_{W_i} = -\dfrac{d_E}{m_i l}\alpha_i$ where $m_i = \pm 1$ and $d_E = gcd(m_i, m') = 1$ for each component. Therefore, the monodromy is

$$\phi = a^p \cdot b^{-(p-1)} \cdot c_1^{-1} \dots c_u^{-1} \cdot d_1^1 \dots d_u^1.$$

Here, a denotes a curve parallel to the boundary component $\{x = 0\}$ and c_i to $\{x^p + \alpha^i y^{p-1} = 0\}$ which are shown as dashed lines in Figure 5.3. We see that the number of negative Dehn twists is $p + u - 1$.

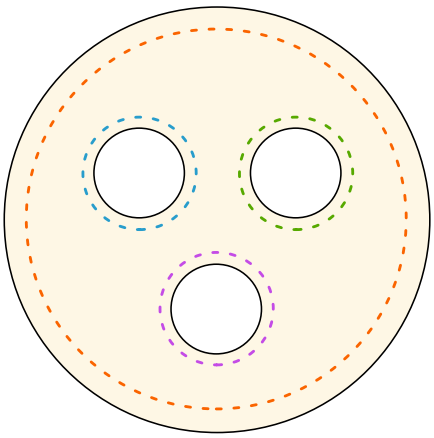

Figure 5.3. 4-punctured sphere corresponding to the case (u=1). The dashed lines indicate the boundaries.

As we discussed in Chapter 4, by the monodromy information of the given open book decomposition, we can construct the corresponding 4-manifold with boundary S^3 and with an achiral Lefschetz fibration to calculate d_3 invariant of a contact structure on S^3 which is compatible with the open book. Since the pages have $(2u+2)$ boundary components, we first attach $(2u+1)$ handles to D^4 to get $D^2 \times \Sigma_{0,2u+2}$. Then, we attach 2-handles along Legendrian copies of the homologically nontrivial curves on $\Sigma_{0,2u+2}$ near the boundaries of the pages with ± 1 framing depending on the parity of Dehn twist. The resulting 4-manifold W is given in Figure 5.4.

Therefore, the 1-chain group $C_1(W)$ has a basis

$$\{X, Y, Z_1, \ldots, Z_{2u-1}\}$$

and $C_2(W)$ has a basis

$$\{a_1, \ldots, a_p, b_1, \ldots, b_{p-1}, c_1, \ldots, c_u, d_1, \ldots, d_u\}.$$

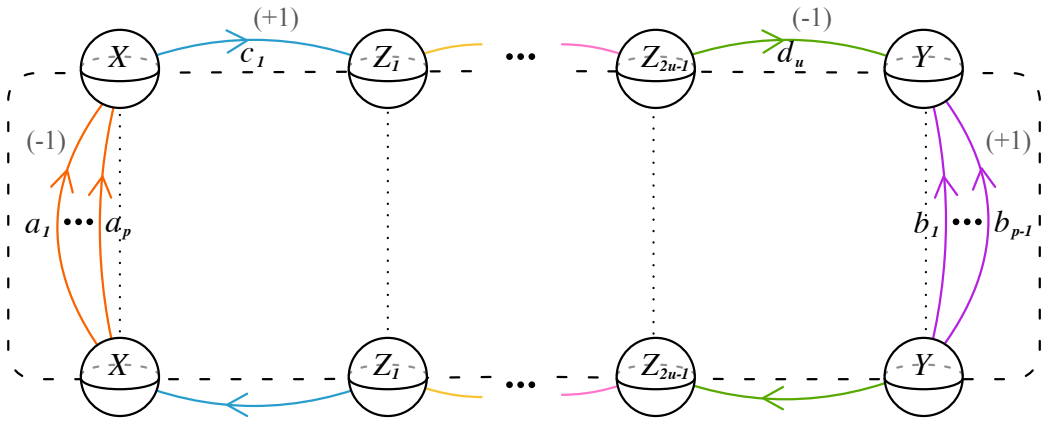

Figure 5.4. Kirby diagram for the 4-manifold corresponding to (I)

The boundary map $D : C_2(W) \to C_1(W)$ is given by $D(a_j) = X$, $D(b_j) = Y$, $D(c_1) = Z_1 - X$, $D(c_i) = Z_i - Z_{i-1}$, $D(d_u) = Y - Z_{2u-1}$, $D(d_i) = Z_{u+i} - Z_{u+i-1}$. Thus, $H_2(W)$ has a basis with generators

$$\{a_1 - a_2, \ldots, a_{p-1} - a_p, b_1 - b_2, \ldots, b_{p-2} - b_{p-1}, b_1 - \sum_{i=1}^{u}(c_i + d_i) - a_p\}.$$

Since $\operatorname{rank} H_0 = 1$, $\operatorname{rank} H_1 = 0$ and $\operatorname{rank} H_2 = 2p - 2$, we get $\chi(W) = 2p - 1$.

Note that, $a_j^2 = -1 = d_j^2$, $b_j^2 = 1 = c_j^2$. So the square of basis elements are $(a_j - a_{j+1})^2 = -2$, $(b_j - b_{j+1})^2 = 2$, $(b_1 - \sum_{i=0}^{u}(c_i + d_i) - a_p)^2 = 0$ and in that basis, the intersection matrix is:

$$Q_W = \left[\begin{array}{ccc|c} & & & \\ & \tilde{J}_{p-1} & & \\ & & & -1 \\ \hline & & & 1 \\ & & J_{p-2} & \\ & & & \\ \hline & -1 & 1 & 0 \end{array}\right]$$

where

$$J_n = \begin{pmatrix} 2 & -1 & 0 & \dots & 0 \\ -1 & 2 & -1 & 0 & \vdots \\ 0 & -1 & \ddots & \dots & 0 \\ \vdots & 0 & \dots & 2 & -1 \\ 0 & \dots & 0 & -1 & 2 \end{pmatrix}_{n\times n} , \tilde{J}_n = \begin{pmatrix} -2 & 1 & 0 & \dots & 0 \\ 1 & -2 & 1 & 0 & \vdots \\ 0 & 1 & \ddots & \dots & 0 \\ \vdots & 0 & \dots & -2 & 1 \\ 0 & \dots & 0 & 1 & -2 \end{pmatrix}_{n\times n}$$

The number of positive eigenvalues and negative eigenvalues of Q are the same and is equal to $p-1$. This follows from Sylvester's Law of Inertia, which says for a symmetric matrix A and some nonsingular matrix W, A and WAW^T have the same number of positive, negative and zero eigenvalues. Therefore, Q and the diagonal matrix D have the same signature. D has diagonal entries $-2, -\frac{3}{2}, \dots, -\frac{p}{p-1}, 2, \frac{3}{2}, \dots, \frac{p-1}{p-2}, \frac{1}{p(p-1)}$. Hence, $\sigma(W) = 0$. Moreover, Since Q is symmetric , Q has the same determinant as D: $\det Q = (-1)^{p-1}$.

To calculate c^2, the square of the first Chern class, note that $rot(a) = 0 = rot(b)$, $rot(c_i) = -1$ and $rot(d_i) = -1$. Let us denote the cocores of the 2-handles attached along a_i, b_j, c_k, d_l by A_i, B_j, C_k, D_l respectively. Then, we see that $c(W)$ is Poincaré

dual to

$$-(\sum_{i=1}^{u} C_i + \sum_{j=1}^{u} D_j).$$

This evaluates on the basis above as $w = (0, \dots, 2u)^T$. Hence,

$$c^2(W) = Q_W(PD(c(W))) = \frac{4u^2 \cdot (-1)^{p-1} \cdot (p-1) \cdot p}{(-1)^{p-1}} = 4u^2 p(p-1).$$

Inserting the results of the previous steps into the formula (4.1) of d_3 invariant, we obtain:

$$\mathrm{d}_3(\xi) = \frac{1}{4}(4u^2(p-1)p - 2(2p-1) - 3 \cdot 0) + p + u - 1 = u^2 p(p-1) + u - \frac{1}{2}.$$

By a similar calculation, we conclude the following information about the other multilinks given in Figure 5.1.

Example 5.2. For $q \in \mathbb{Z}^+$, consider

$$f\overline{g} = x\overline{y} \prod_{i=1}^{u} (x^q + \alpha^i y) \prod_{j=1}^{u-1} \overline{(x^q + \alpha^{u+j} y)}.$$

Following the steps in the previous example, we see that the singularity link of this real analytic map corresponds to the splice diagram (II) in Figure 5.1 which is a fibered with trivial monodromy and the Milnor fibration has planar pages like the previous example. For the compatible contact structure, we have

$$\mathrm{d}_3(\xi) = \frac{1}{4}((2u-1)^2 q - 2(q+1) - 3q) + q + u = u(u-1)q + u - \frac{1}{2}.$$

Example 5.3. Consider

$$f\overline{g} = \overline{xy} \prod_{i=1}^{u+1} (x^3 + \alpha^i y^2) \prod_{j=1}^{u} \overline{(x^3 + \alpha^{u+j+1} y^2)}.$$

Similarly as before, we see that singularity link of this real analytic map corresponds to the splice diagram (III) in Figure 5.1 which is fibered with trivial monodromy and the Milnor fibration has planar pages as before. For the compatible contact structure, we have

$$\mathrm{d}_3(\xi) = \frac{1}{4}(6(2u+1)^2 - 2\cdot 5 - 3\cdot(-2)) + u + 1 = 6u(u+1) + u + 2 - \frac{1}{2}.$$

In Chapter 3, we discussed that if the splice components of a graph multilink is fibered then it is fibered too. While splicing two multilinks, we paste the corresponding Seifert surfaces along their boundary on the splicing torus. Thus, when we splice fibered Seifert multilinks with planar pages, the resulting multilink is still fibered and has planar pages. Therefore, we can use Seifert multilinks with planar fibers as building blocks to construct new fibered multilinks with planar fibers. However, we should note that splicing is not possible all the time and it should satisfy the cohomology condition (3.4). Moreover, when each splice component corresponds to a real analytic singularity, we consider the real analytic maps where we obtain by omitting the branches corresponding to the link components on which splicing occurs. The product of these maps corresponds to the multilink obtained via splicing.

Now, we explain the splicing possibilities of the multilinks given in Figure 5.1 and the possible outcomes of the splicing operations; we omit the detailed calculations. For the Seifert multilink in Figure 5.1, there are various possible ways to splice. However, we consider splicing along the link component with weight p where the link component, it is spliced with, must have multiplicity 1, along the link component with weight $p-1$ where the opposite splice component must have multiplicity -1 for the Seifert multilinks (I). For the Seifert multilink (II), we consider splicing along the components with weight 1 when $q = 2$. For the Seifert multilink (III), splicing is possible only along the component with weight 3 which can be spliced with a link component with multiplicity 1. We summarize the possible multilinks with planar fibers that can be obtained by splicing the given Seifert multilinks.

Lemma 5.1. *We can obtain infinite families of real algebraic overtwisted contact structures on S^3 supported by planar open books which has bindings obtained by splicing:*

- $(I) - \cdots - (I)$
- $(II) - (I) - \cdots - (I)$
- $(III) - (I) - \cdots - (I)$

We will only consider the infinite family of fibered graph multilinks which are of the form (I)-(I) and (I)-(I)-(I).

Example 5.4. In this example, we construct the contact structures corresponding to the multilinks we obtained via splicing real analytic singularity multilinks (I)-(I) given in Example 5.1.

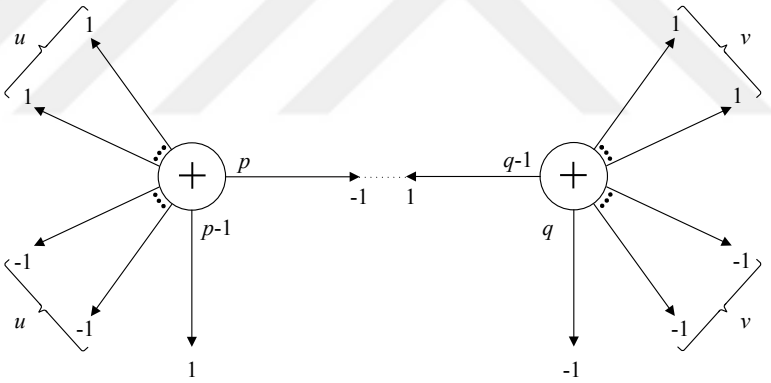

Figure 5.5. Splice diagram for (I)-(I)

We splice the link component corresponding to $\{\bar{x} = 0\}$ of the former splice component to the link component corresponding to $\{y = 0\}$ of the latter splice component. Because, the splice link has multiplicity $m_1 = -1(1 \cdots 1) + v \cdot 1 \cdot q + v \cdot (-1) \cdot q = -1$ and $m_2 = 1(1 \cdots 1) + u \cdot 1 \cdot (p-1) + u \cdot (-1) \cdot (p-1) = 1$ which agree with the multiplicity -1 of $\{\bar{x} = 0\}$ component of the first link and the multiplicity 1 of $\{y = 0\}$ component of the second link, this splicing is valid. Moreover, by omitting the branches of the singularities corresponding to the splice components, we see that the multilink we got

after splicing corresponds to the real analytic map of the form $f\overline{g}$ given below:

$$\overline{x}y\prod_{i=1}^{u}(x^p+\alpha^i y^{p-1})\prod_{k=1}^{v}(x^q+\alpha^k y^{q-1})\prod_{j=u+1}^{2u}\overline{(x^p+\alpha^j y^{p-1})}\prod_{l=v+1}^{2v}\overline{(x^q+\alpha^l y^{q-1})}.$$

By Example 5.1, we know that $l_1 = l_2 = 1$. And also, $d_E = (m_1, m_2) = 1$. Thus $t_W = -\dfrac{d_E}{l_1 l_2}(p(q-1) - q(p-1)) = p - q$. If we assume that $q > p$, then $t_W < 0$.

We can express the page of the splice link as a union of the pages of the splice components joined together from a boundary by a $p - q$ twisted toral annulus (since $d_E = 1$). Since the splice components have $2u + 2$ and $2v + 2$-punctured sphere pages, the pages for the splice link are $2u + 2v + 2$-punctured spheres, see Figure 5.6.

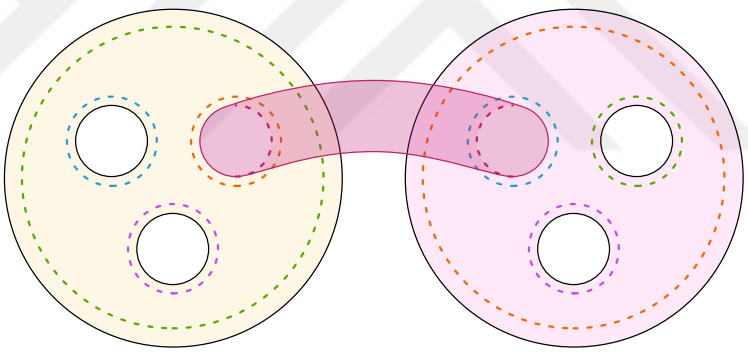

Figure 5.6. Pages for (I)-(I) corresponding to the case $(u = 1, v = 1)$

When we splice two multilinks, we glue boundary components of both links which correspond to the link components we splice. Hence, after splicing, the Dehn twists corresponding to glued boundaries becomes nullhomologous in the link exterior, i.e. there is no contribution to the monodromy from spliced boundary components. Moreover, because of the monodromy flow in each end of the connecting annulus, monodromy has $-(q - p)$ twists. Recall that the monodromy maps are $\phi_1 = \alpha^p \cdot a^{-(p-1)} \cdot c_1^{-1} \dots c_u^{-1} \cdot d_1^1 \dots d_u^1$ and $\phi_2 = b^q \cdot \beta^{-(q-1)} \cdot e_1^{-1} \dots e_v^{-1} \cdot f_1^1 \dots f_v^1$ in the splice components. Therefore, we conclude that the monodromy of the new fibration

is $\phi = a^{-(p-1)} \cdot c_1^{-1} \cdots c_u^{-1} \cdot d_1^1 \cdots d_u^1 \cdot \gamma^{-k} \cdot b^q \cdot e_1^{-1} \cdots e_v^{-1} \cdot f_1^1 \cdots f_v^1$ where $k = q - p$. Thus, the number of negative Dehn twists is $q + u + v - 1$.

Similarly as before, we can use the monodromy data to construct a 4-manifold with boundary S^3 admitting an achiral Lefschetz fibration, which induces the open book decomposition on the boundary. Because the pages have $(2u + 2v + 2)$ boundary components, first of all, we attach $(2u + 2v + 1)$ handles to D^4 to get $D^2 \times \Sigma_{0,2u+2v+2}$. Since the monodromy is obtained by the monodromies of the splice components, to construct the 4-manifold, we can use the Kirby diagrams for the splice components. Next, we attach 2-handles along the Legendrian copies of the homologically nontrivial curves on $\Sigma_{0,2u+2v+2}$ near the boundaries of the pages with ± 1 framing as before and add one more 2-handle corresponding to the monodromy flow on the separating annulus depending on the parity of the twist. Consequently, the resulting 4-manifold W is given in Figure 5.7.

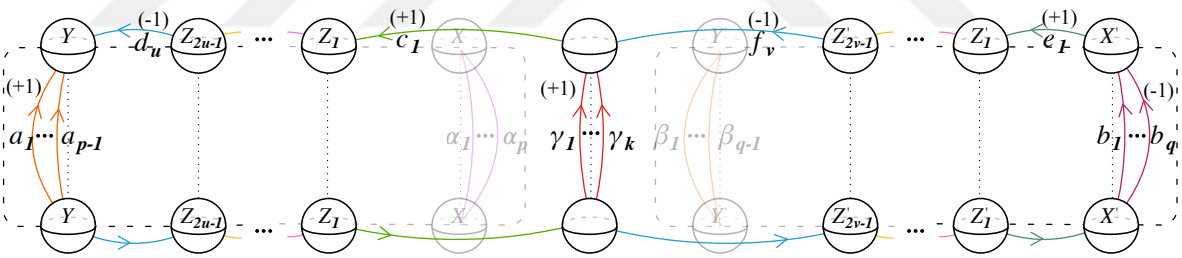

Figure 5.7. Kirby diagram for the 4-manifold corresponding to (I)-(I)

Furthermore, $H_2(W)$ has a basis with generators:

$$a_1 - a_2, \ldots, a_{p-2} - a_{p-1}, \gamma_1 - \gamma_2, \ldots, \gamma_{k-1} - \gamma_k, b_1 - b_2, \ldots, b_{q-1} - b_q,$$
$$\gamma_1 + (\sum_{i=1}^{u} c_i + d_i) - a_{p-1}, b_1 + (\sum_{i=1}^{v} e_i + f_i) - \gamma_k.$$

Since rank $H_0 = 1$, rank $H_1 = 0$ and rank $H_2 = 2q - 2$, consequently, we have $\chi(W) = 2q - 1$.

Note that, $a_j^2 = c_j^2 = e_j^2 = \gamma_j^2 = 1$ and $b_j^2 = d_j^2 = f_j^2 = -1$. So the squares of the basis elements are $(a_j - a_{j+1})^2 = 2$, $(\gamma_j - \gamma_{j+1})^2 = 2$, $(b_j - b_{j+1})^2 = -2$, $(\gamma_1 + (\sum_{i=1}^{u} c_i + d_i) - a_{p-1})^2 = 2$ and $(b_1 + (\sum_{i=1}^{v} e_i + f_i) - \gamma_k)^2 = 0$. In this basis, the intersection matrix is:

$$Q_W = \left(\begin{array}{ccc|c} & & & \\ \multicolumn{1}{c}{J_{p-2}} & & & \multicolumn{1}{c}{1} \\ \hline & & & 1 \\ & J_{q-p-1} & & \multicolumn{1}{c}{1} \\ \hline & & & -1 \\ & & \tilde{J}_{q-1} & \\ \hline 1 & 1 & & 2 \\ & & 1 \quad -1 & 0 \end{array}\right)$$

Q_W can be seen as the block matrix in the form:

$$\left[\begin{array}{c|c} A & B^T \\ \hline B & C \end{array}\right]$$

where A, B, C are $(2q-4) \times (2q-4)$, $2 \times (2q-4)$ and 2×2 symmetric matrices respectively..

Since Q_W is symmetric , there is an orthogonal matrix S such that SQ_WS^T is diagonal. Let S_1 and S_2 be the orthogonal matrices diagonalize A and $C - BA^{-1}B^T$ respectively. Define

$$S = \left[\begin{array}{c|c} P_1 & 0 \\ \hline -P_2BA^{-1} & P_2 \end{array}\right].$$

It can be seen easily that

$$SQS^T = \left[\begin{array}{c|c} P_1AP_1^T & 0 \\ \hline 0 & P_2(C - BA^{-1}B^T)P_2^T \end{array}\right].$$

Hence,

$$\sigma(Q_W) = \sigma(SQ_WS^T) = \sigma(P_1AP_1^T)+\sigma(P_2(C-BA^{-1}B^T)P_2^T) = \sigma(A)+\sigma(C-BA^{-1}B^T).$$

We know that J_n and $\tilde{J}_n$ are diagonalizable and are positive definite and negative definite respectively. Therefore, A has $(p-2)+(q-p-1) = q-3$ positive and $q-1$ negative eigenvalues. It can be easily seen that $C - BA^{-1}B^T$ is positive definite, hence has 2 positive eigenvalues. Thus, $\sigma(W) = 0$.

Moreover, we have $\det Q_W = (-1)^{q-1}$ which is calculated in Appendix A.

Note that, $rot(a) = rot(\gamma) = rot(b) = 0$, $rot(c_i) = -1$, $rot(d_i) = -1$, $rot(e_i) = -1$ and $rot(f_i) = -1$. Then, $c(W) = -\sum_{i=1}^{u}(C_i + D_i) - \sum_{j=1}^{v}(E_j + F_j)$. This evaluates on the basis above as $w = (0, \ldots, -2u, -2v)^T$. In order to calculate c^2, it is sufficient to calculate the inverse of last 2×2 block of Q_W. We deduce that $c^2(W) = 4u^2p(p-1) + 8uvq(p-1) + 4v^2q(q-1)$. Explicit calculations can be found in Appendix A.

Inserting the results of the previous steps into the formula of the invariant d_3, we obtain:

$$\begin{aligned}\mathrm{d}_3(\xi) &= \frac{1}{4}(4u^2p(p-1) + 8uvq(p-1) + 4v^2q(q-1) - 2(2q-1) - 3\cdot 0) + q + u + v - 1 \\ &= u^2p(p-1) + v^2q(q-1) + 2uvq(p-1) + u + v - \frac{1}{2}.\end{aligned}$$

As we have seen, the information about the resulting graph link and its fibration can be deduced from the splice components easily. Continuing the same procedure, we

can construct new families of open book decompositions, hence new contact structures. In the next example, we will construct a wider family of overtwisted contact structures and observe how the procedure goes on.

Example 5.5. Similarly as in the previous example, we can splice three multilinks given in Example 5.1. In other words, we can splice the multilink in Example 5.1 with the multilink in Example 5.2 and the resulting splice multilink is given by the diagram in Figure 5.8. We splice the link component corresponding to $\{\bar{x} = 0\}$ of the first

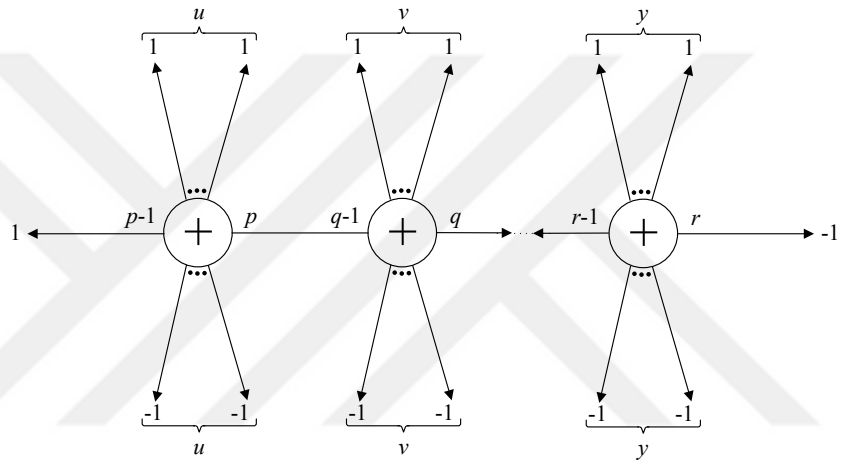

Figure 5.8. Splice diagram for (I)-(I)-(I)

splice component to the link component corresponding to $\{y = 0\}$ of the second splice component as in the previous example. As we discussed before, it can be easily seen that this splicing is valid. By the previous examples, we know that $l_1 = l_2 = 1$. And also, $d_E = (m_1, m_2) = 1$. Thus the $t_W = -\frac{d_E}{l_1 l_2}(q(r-1) - r(q-1) = q - r$. If we assume that $r > q$, $t_W < 0$.

We can express the page of the splice multilink as a union of the pages of the splice components joined together from a boundary by a $q - r$ twisted toral annulus (since $d_E = 1$). Since our splice components has $2u + 2v + 2$ and $2y + 2$-punctured sphere pages, the pages for the splice link are $2u + 2v + 2y + 2$-punctured sphere.

The monodromy of the new fibration is

$$\phi = a^{-(p-1)}c_1^{-1}\cdots c_u^{-1}d_1^1\cdots d_u^1\gamma^{-(q-p)}e_1^{-1}\cdots e_v^{-1}f_1^1\cdots f_v^1\theta^{-(r-q)}b^r g_1^{-1}\cdots g_y^{-1}h_1^1\cdots h_y^1.$$

Hence, the number of negative Dehn twists is $r+u+v+y-1$.

By the same arguments as in the previous example, the corresponding 4-manifold has the following Kirby diagram given in Figure 5.9

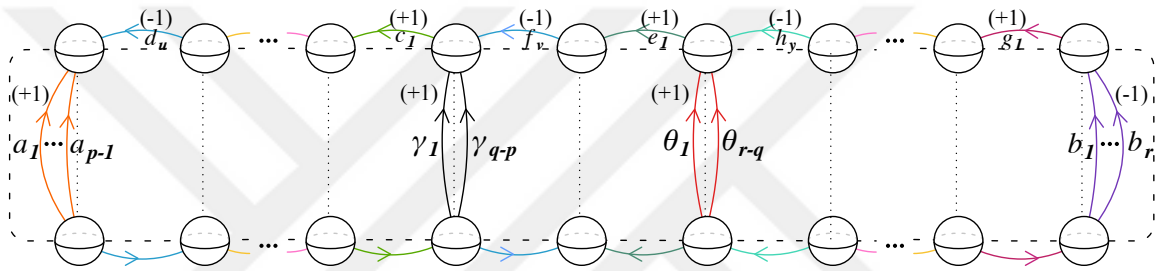

Figure 5.9. Kirby diagram for the 4-manifold corresponding to (I)-(I)-(I)

$H_2(W)$ has a basis with generators:

$$a_1-a_2,\ldots,a_{p-2}-a_{p-1},\gamma_1-\gamma_2,\ldots,\gamma_{q-p-1}-\gamma_{q-p},\theta_1-\theta_2,\ldots,\theta_{r-q-1}-\theta_{r-q},$$
$$b_1-b_2,\ldots,b_{r-1}-b_r,\gamma_1+(\sum_{i=1}^{u}c_i+d_i)-a_{p-1},$$
$$\theta_1+(\sum_{i=1}^{v}e_i+f_i)-\gamma_{q-p},b_1+(\sum_{i=1}^{y}g_i+h_i)-\theta_{r-q}.$$

Since rank $H_0=1$, rank $H_1=0$ and rank $H_2=2r-2$, we have $\chi(W)=2r-1$.

Note that, $a_j^2=c_j^2=e_j^2=g_j^2=\gamma_j^2=\theta_j^2=1$ and $b_j^2=d_j^2=f_j^2=h_j^2=-1$. So the squares of the basis elements are $(a_j-a_{j+1})^2=2$, $(\gamma_j-\gamma_{j+1})^2=2$, $(\theta_j-\theta_{j+1})^2=2$, $(b_j-b_{j+1})^2=-2$, $(\gamma_1-(\sum_{i=1}^{u}c_i+d_i)-a_{p-1})^2=2$, $(\theta_1-(\sum_{i=1}^{v}e_i+f_i)-\gamma_{q-p})^2=2$ and $(b_1-(\sum_{i=1}^{y}g_i+h_i)-\theta_{r-q})^2=0$. In this basis, the intersection matrix is:

$$Q_W = \left(\begin{array}{c|c|c|c|c} J_{p-2} & & & & 1 \\ \hline & J_{q-p-1} & & & \begin{matrix}1 \\ & 1\end{matrix} \\ \hline & & J_{r-q-1} & & \begin{matrix}1 & \\ & 1\end{matrix} \\ \hline & & & \tilde{J}_{r-1} & \begin{matrix} & -1 \\ & \end{matrix} \\ \hline \begin{matrix} & 1 \\ & \end{matrix} & \begin{matrix}1 & \\ & \end{matrix} & \begin{matrix} & \\ 1 & 1 \end{matrix} & \begin{matrix} & \\ & \end{matrix} & \begin{matrix}2 & \\ & 2 \\ & \end{matrix} \\ & & \begin{matrix} & \\ & \end{matrix} & \begin{matrix} & \\ 1 & -1 \end{matrix} & \begin{matrix} & \\ & 0 \end{matrix} \end{array}\right).$$

The number of positive eigenvalues is $(p-2)+(q-p-1)+(r-q-1)+3 = r-1$ and the number of negative eigenvalues is $(r-1)$ as we discussed in the previous example. Thus, $\sigma(W) = 0$. Furthermore, $\det Q_W = (-1)^{r-1}$.

Note that, $rot(a) = rot(b) = rot(\gamma) = rot(\theta) = 0$, whereas $rot(c_i) = -1$, $rot(d_i) = -1$, $rot(e_i) = -1$, $rot(f_i) = -1$, $rot(g_i) = -1$ and $rot(h_i) = -1$. Therefore, we have $c(W) = -\sum_{i=1}^{u}(C_i + D_i) - \sum_{j=1}^{v}(E_j + F_j) - \sum_{j=1}^{y}(G_j + H_j)$. This evaluates on the basis above as $w = (0, \ldots, -2u, -2v, -2y)^T$. In order to calculate c^2, it is sufficient to calculate the inverse of the last 3×3 block of Q_W. By following the calculations in

Appendix A, we observe

$$c^2(W) = (-2u,-2v,-2y)\begin{pmatrix} p(p-1) & q(p-1) & r(p-1) \\ q(p-1) & q(q-1) & r(q-1) \\ r(p-1) & r(q-1) & r(r-1) \end{pmatrix}(-2u,-2v,-2y)^T$$
$$= 4u^2p(p-1) + 4v^2q(q-1) + 4y^2r(r-1)$$
$$+ 8uvq(p-1) + 8uyr(p-1) + 8vyr(q-1).$$

Therefore, inserting the results we obtained in the previous steps into the formula of the invariant d_3, we have:

$$\mathrm{d}_3(\xi) = \frac{1}{4}\begin{pmatrix} 4u^2p(p-1) + 4v^2q(q-1) + 4y^2r(r-1) + 8uvq(p-1) \\ + 8uyr(p-1) + 8vyr(q-1) - 2\cdot(2r-1) - 3\cdot(0) \end{pmatrix}$$
$$+ r + u + v + y - 1$$
$$= u^2p(p-1) + v^2q(q-1) + y^2r(r-1) + 2uvq(p-1)$$
$$+ 2uyr(p-1) + 2vyr(q-1) + u + v + y - \frac{1}{2}.$$

After these results, we have reached to the following conclusion about the constructions of the real algebraic overtwisted contact structures supported by planar open books.

Theorem 5.2. *All overtwisted contact structures on S^3 with $\mathrm{d}_3 > 0$ are supported by planar open book decompositions induced by real algebraic functions of the form $f\overline{g}$. Furthermore, the family of fibered multilinks we obtained in Example 5.5 with $u = v = y = 1$ gives us all the overtwisted contact structures where $\mathrm{d}_3 + \frac{1}{2} > 0$ is odd, whereas $u = 2$, $v = y = 1$ gives us all the ones where $\mathrm{d}_3 + \frac{1}{2} > 0$ is even.*

Proof. When $u = v = y = 1$, we have

$$\mathrm{d}_3 + \frac{1}{2} = p(p-1) + q(q-1) + r(r-1) + 2q(p-1) + 2r(p-1) + 2r(q-1) + 3.$$

It is clear that $p(p-1)+q(q-1)+r(r-1)+2q(p-1)+2r(p-1)+2r(q-1)$ is of the form $2M$ and we want to show that we can find triples (p,q,r) for all $M \geq 0$. After some simplification, we see that

$$2M = (p+q+r)^2 - p - 3q - 5r.$$

For $M = 0$, the equation holds when $(p,q,r) = (0,3,0)$. For the inductive step, consider the following operations:

(i) if $q \geq 1$, the triple $(p+1, q-1, r)$ gives $2(M+1)$,
(ii) if $p \geq 1$, the triple $(p-1, q+2, r)$ gives $2(M+p+q+r-4)$.

We will show that starting from $2M = 0$ we can obtain all positive even integers with these operations. We observe that if $2M$ is of the form k^2+3k, the equation holds when $(p,q,r) = (0,k+3,0)$. By applying the operation (i), we have the triple $(1,k+2,0)$ and the equation holds for $k^2+3k+2 = 2(M+1)$. By applying the operation (ii) to this triple, we get $(0,k+4,0)$ which satisfies the equation for $(k+1)^2+3(k+1)$. Any even integer in between can be obtained by successively applying the operation (i) to the triple $(1,k+2,0)$.

By repeating the same procedure on $(0,k+4,0)$ and so on, we can obtain all positive even integers by applying steps (i), (ii) and the sequence of (i)'s.

Similarly, for the multilinks with $u = 2$, $v = y = 1$, we have

$$\mathrm{d}_3 + \frac{1}{2} = 4p(p-1) + q(q-1) + r(r-1) + 4q(p-1) + 4r(p-1) + 2r(q-1) + 4.$$

Again, it is clear that it is of the form $2M$ and we want to show that it can generate all the positive even integers. After some simplifications, the equation turns out

$$2M = (2p+q+r)^2 - 4p - 5q - 7r.$$

When $(p, q, r) = (0, 0, 7)$, it is equal to 0. For the inductive step, consider the following operations:

(i) if $r \geq 1$, the triple $(p, q + 1, r - 1)$ gives $2(M + 1)$,
(ii) if $q \geq 1$, the triple $(p, q - 1, r + 2)$ gives $2(M + p + q + r - 4)$.

Following the same procedure, we will show that we can obtain all positive even integers with these operations. We observe that if $2M$ is of the form k^2+7k, the equation holds when $(p, q, r) = (0, 0, k+7)$. By applying the operation (i), we have the triple $(0, 1, k+6)$ and the equation holds for $k^2 + 7k + 2 = 2(M + 1)$. By applying the operation (ii) to this triple, we get $(0, 0, k + 8)$ which satisfies the equation for $(k + 1)^2 + 7(k + 1)$. Any even integer in between can be obtained by successively applying the operation (i) to the triple $(1, k + 2, 0)$. Therefore, we can generate all the positive integers by $\mathrm{d}_3 + \frac{1}{2}$ where $u = v = y = 1$ and $u = 2$, $v = y = 1$.

6. CONCLUSION

In this thesis, we constructed some families of real analytic maps with an isolated singularity at the origin and showed that the corresponding singularity links are multilinks in S^3 which are bindings of the planar open books supporting overtwisted contact structures with positive d_3 invariants. It is still an open question that whether the overtwisted contact structures with negative d_3 invariants can be obtained as singularity links. It is known that every overtwisted contact structure is supported by a planar open book decomposition. Thus a further question to consider is whether overtwisted contact structures with $d_3 < 0$ are supported by planar open book decompositions with real analytic bindings. If the answer is negative, the next question might be whether they can be obtained by open book decompositions with real analytic bindings and pages of minimum genus. Another question that can be asked is whether any overtwisted contact structure in an arbitrary 3-manifold is real algebraic.

Splicing multilinks is an algebraic operation whose effect on the germs of the functions can be read off easily. A further question to be considered is to find an algebraic operation in 4-manifold which corresponds to the splicing operation on the boundary of the manifold. Finding such operation would simplify to describe the 4-manifold which we obtained after splicing by means of the spliced 4-manifolds and calculate the d_3 invariant of the corresponding contact structure.

REFERENCES

1. Eliashberg, Y., "Classification of overtwisted contact structures on 3-manifolds", *Invent. Math.*, Vol. 98, No. 3, pp. 623–637, 1989.

2. Gromov, M., "Pseudo holomorphic curves in symplectic manifolds", *Invent. Math.*, Vol. 82, No. 2, pp. 307–347, 1985.

3. Eliashberg, Y., "Filling by holomorphic discs and its applications", *Geometry of low-dimensional manifolds, 2 (Durham, 1989)*, Vol. 151 of *London Math. Soc. Lecture Note Ser.*, pp. 45–67, Cambridge Univ. Press, Cambridge, 1990.

4. Ozbagci, B. and A. I. Stipsicz, *Surgery on contact 3-manifolds and Stein surfaces*, Vol. 13 of *Bolyai Society Mathematical Studies*, Springer-Verlag, Berlin; János Bolyai Mathematical Society, Budapest, 2004.

5. Caubel, C., A. Némethi and P. Popescu-Pampu, "Milnor open books and Milnor fillable contact 3-manifolds", *Topology*, Vol. 45, No. 3, pp. 673–689, 2006.

6. Varčenko, A. N., "Contact structures and isolated singularities", *Vestnik Moskov. Univ. Ser. I Mat. Mekh.*, Vol. 35, No. 2, pp. 18–21, 101, 1980.

7. Milnor, J., *Singular points of complex hypersurfaces*, Annals of Mathematics Studies, No. 61, Princeton University Press, Princeton, N.J.; University of Tokyo Press, Tokyo, 1968.

8. Giroux, E., "Géométrie de contact: de la dimension trois vers les dimensions supérieures", *Proceedings of the International Congress of Mathematicians, Vol. II*, pp. 405–414, Higher Ed. Press, Beijing, 2002.

9. Etnyre, J. B., "Lectures on open book decompositions and contact structures", *Floer Homology, Gauge Theory, and Low-Dimensional Topology: Proceedings of*

the Clay Mathematics Institute 2004 Summer School, Alfréd Rényi Institute of Mathematics, Budapest, Hungary, June 5-26, 2004, Vol. 5, p. 103, American Mathematical Soc., 2006.

10. A'Campo, N., "Le nombre de Lefschetz d'une monodromie", *Indagationes Mathematicae (Proceedings)*, Vol. 76, pp. 113–118, Elsevier, 1973.

11. Ruas, M. A. S., J. Seade and A. Verjovsky, "On real singularities with a Milnor fibration", *Trends in singularities*, Vol. 21 of *Trends in Mathematics*, pp. 191–213, 2002.

12. Pichon, A. and J. Seade, "Fibred multilinks and singularities $f\overline{g}$", *Math. Ann.*, Vol. 342, No. 3, pp. 487–514, 2008.

13. Pichon, A., "Real analytic germs and open-book decompositions of the 3-sphere", *International Journal of Mathematics*, Vol. 16, No. 01, pp. 1–12, 2005.

14. Pichon, A. and J. Seade, "Real singularities and open-book decompositions of the 3-sphere", *Annales de la Faculté des sciences de Toulouse: Mathématiques*, Vol. 12, pp. 245–265, 2003.

15. Rudolph, L., "Isolated critical points of mappings from R^4 to R^2 and a natural splitting of the Milnor number of a classical fibered link. Part I: Basic theory; examples", *Commentarii Mathematici Helvetici*, Vol. 62, No. 1, pp. 630–645, 1987.

16. Ishikawa, M., "Compatible Contact Structures of Fibered Positively Twisted Graph Multilinks in the 3-Sphere", *Vietnam Journal of Mathematics*, Vol. 42, No. 3, pp. 273–293, 2014.

17. Perron, B., "Le noeud "Huit" est Algebrique Réel", *Inventiones mathematicae*, Vol. 65, No. 3, pp. 441–451, 1982.

18. Ishikawa, M., "Compatible contact structures of fibered Seifert links in homology

3-spheres", *Tohoku Math. J. (2)*, Vol. 64, No. 1, pp. 25–59, 2012.

19. Eisenbud, D. and W. Neumann, *Three-dimensional link theory and invariants of plane curve singularities*, Vol. 110 of *Annals of Mathematics Studies*, Princeton University Press, Princeton, NJ, 1985.

20. Etnyre, J. B. and B. Ozbagci, "Invariants of contact structures from open books", *Trans. Amer. Math. Soc.*, Vol. 360, No. 6, pp. 3133–3151, 2008.

21. Seade, J., *On the topology of isolated singularities in analytic spaces*, Vol. 241 of *Progress in Mathematics*, Birkhäuser Verlag, Basel, 2006.

22. Némethi, A., "Five lectures on normal surface singularities", *Low dimensional topology (Eger, 1996/Budapest, 1998)*, Vol. 8 of *Bolyai Soc. Math. Stud.*, pp. 269–351, 1999.

23. Brieskorn, E. and H. Knörrer, *Plane algebraic curves*, Modern Birkhäuser Classics, Birkhäuser/Springer Basel AG, Basel, 1986.

24. Neumann, W. D., "A calculus for plumbing applied to the topology of complex surface singularities and degenerating complex curves", *Trans. Amer. Math. Soc.*, Vol. 268, No. 2, pp. 299–344, 1981.

25. Seade, J., "On Milnor's fibration theorem and its offspring after 50 years", *Bull. Amer. Math. Soc. (N.S.)*, Vol. 56, No. 2, pp. 281–348, 2019.

26. Jankins, M. and W. D. Neumann, *Lectures on Seifert manifolds*, Vol. 2 of *Brandeis Lecture Notes*, Brandeis University, Waltham, MA, 1983.

27. Neumann, W. D. and F. Raymond, "Seifert manifolds, plumbing, μ-invariant and orientation reversing maps", *Algebraic and geometric topology (Proc. Sympos., Univ. California, Santa Barbara, Calif., 1977)*, Vol. 664 of *Lecture Notes in Math.*, pp. 163–196, Springer, Berlin, 1978.

28. Neumann, W. D., "Splicing algebraic links", *Complex analytic singularities*, Vol. 8 of *Adv. Stud. Pure Math.*, pp. 349–361, North-Holland, Amsterdam, 1987.

29. Akbulut, S. and H. King, "All knots are algebraic", *Comment. Math. Helv.*, Vol. 56, No. 3, pp. 339–351, 1981.

30. Eliashberg, Y., "Contact 3-manifolds twenty years since J. Martinet's work", *Ann. Inst. Fourier (Grenoble)*, Vol. 42, No. 1-2, pp. 165–192, 1992.

31. Turaev, V. G., "Euler structures, nonsingular vector fields, and torsions of Reidemeister type", *Mathematics of the USSR-Izvestiya*, Vol. 34, No. 3, p. 627, 1990.

32. Gompf, R. E., "Handlebody construction of Stein surfaces", *Ann. of Math. (2)*, Vol. 148, No. 2, pp. 619–693, 1998.

33. Harer, J., "How to construct all fibered knots and links", *Topology*, Vol. 21, No. 3, pp. 263–280, 1982.

34. Ding, F. and H. Geiges, "A Legendrian surgery presentation of contact 3-manifolds", *Math. Proc. Cambridge Philos. Soc.*, Vol. 136, No. 3, pp. 583–598, 2004.

35. Ding, F., H. Geiges and A. I. Stipsicz, "Surgery diagrams for contact 3-manifolds", *Turkish J. Math.*, Vol. 28, No. 1, pp. 41–74, 2004.

36. Gompf, R. E. and A. I. Stipsicz, 4-*manifolds and Kirby calculus*, Vol. 20 of *Graduate Studies in Mathematics*, American Mathematical Society, Providence, RI, 1999.

37. Lekili, Y., "Planar open books with four binding components", *Algebr. Geom. Topol.*, Vol. 11, No. 2, pp. 909–928, 2011.

38. Etnyre, J. B., "Planar open book decompositions and contact structures", *Int. Math. Res. Not.*, , No. 79, pp. 4255–4267, 2004.

APPENDIX A: INTERSECTION MATRIX CALCULATIONS

Here, we will give detailed calculations for the results about the intersection matrices we used in Chapter 5. In the splicing of (I)-(I), we have the following intersection matrix:

$$Q = \left(\begin{array}{ccc|c} & & & \\ J_{p-2} & & & 1 \\ \hline & & & 1 \\ & J_{q-p-1} & & \\ & & & 1 \\ \hline & & & -1 \\ & & \tilde{J}_{q-1} & \\ & & & \\ \hline 1 & 1 & & 2 \\ & & 1 \quad -1 & \quad 0 \end{array}\right)$$

where

$$J_n = \begin{pmatrix} 2 & -1 & 0 & \dots & 0 \\ -1 & 2 & -1 & 0 & \vdots \\ 0 & -1 & \ddots & \dots & 0 \\ \vdots & 0 & \dots & 2 & -1 \\ 0 & \dots & 0 & -1 & 2 \end{pmatrix}_{n\times n}, \tilde{J}_n = \begin{pmatrix} -2 & 1 & 0 & \dots & 0 \\ 1 & -2 & 1 & 0 & \vdots \\ 0 & 1 & \ddots & \dots & 0 \\ \vdots & 0 & \dots & -2 & 1 \\ 0 & \dots & 0 & 1 & -2 \end{pmatrix}_{n\times n}$$

Here, we have $\det Q = (-1)^{q-1}$. By induction, it can be easily seen that

$$\det J_n = 2\det J_{n-1} - \det J_{n-2} = n+1,$$

and

$$\det \tilde{J}_n = (-1)^n(n+1).$$

Let J'_n be the matrix obtained by removing the last column of the matrix J_n and J''_n be the matrix obtained by removing the first column of J_n. By calculating the determinant via the last row, it is equal to the the sum of the below determinants multiplied by $(-1)^{q-1}$

$$\begin{vmatrix} J_{p-2} & & & 1 \\ & J'_{q-p-1} & & 1 \\ & & & -1 \\ & & \tilde{J}_{q-1} & \\ 1 & 1 & & 2 \end{vmatrix} + \begin{vmatrix} J_{p-2} & & & 1 \\ & J_{q-p-1} & & 1 \\ & & & -1 \\ & & \tilde{J}''_{q-1} & \\ 1 & 1 & & 2 \end{vmatrix}$$

We replace the last column to the positions of the removed columns, i.e. in the first matrix, we move the $(2q-3)^{rd}$ column to the $(q-3)^{rd}$ column position and in the second matrix to the $(q-2)^{nd}$ column position. These row exchanges multiply the determinants by $(-1)^{(2q-3-q+3)}$ and $(-1)^{(2q-3-q+2)}$, respectively. Since

$$\begin{vmatrix} J'_n & \\ & 1 \end{vmatrix} = \det J_{n-1}, \quad \begin{vmatrix} -1 & \\ & \tilde{J}''_n \end{vmatrix} = -\det \tilde{J}_{n-1} = (-1)^n n,$$

we have

$$\begin{aligned}\det Q = \quad & (-1)^{q-1}\begin{pmatrix} (-1)^{q-1}\cdot\det J'_{p-2}\cdot\det J'_{q-p-1}\cdot\tilde{J}_{q-1} \\ +(-1)^{q-1}\cdot\det J_{p-2}\cdot\det J'''_{q-p-1}\cdot\det\tilde{J}_{q-1} \\ +(-1)^{q}\cdot 2\cdot\det J_{p-2}\cdot\det J'_{q-p-1}\cdot\det\tilde{J}_{q-1}\end{pmatrix} \\ & +(-1)^{q-1}\begin{pmatrix} (-1)^{q}\cdot\det J'_{p-2}\cdot\det J_{q-p-1}\cdot\tilde{J}''_{q-1} \\ +(-1)^{q}\cdot\det J_{p-2}\cdot\det J''_{q-p-1}\cdot\det\tilde{J}''_{q-1} \\ +(-1)^{q-1}\cdot 2\cdot\det J_{p-2}\cdot\det J_{q-p-1}\cdot\det\tilde{J}''_{q-1}\end{pmatrix} \\ & = (-1)^{q}q(q-2)-(-1)^{q}(q-1)^2 \\ & = (-1)^{q-1}.\end{aligned}$$

Moreover, as we see in the same example, $c(W)$ evaluates on the given basis of $H_2(W;\mathbb{Z})$ as $w=(0,\ldots,-2u,-2v)^T$. Hence, in order to calculate c^2, it is sufficient to calculate the inverse of the last 2×2 block of Q. Let's call this matrix D and let d_{ij} be the (i,j) entry.

$$d_{11}=\frac{\mathrm{cofac}_{11}}{\det Q}=p(p-1),\quad d_{12}=d_{21}=q(p-1)\text{ and }d_{22}=q(q-1).$$

In fact,

$$\operatorname{cofac}_{11} = \begin{vmatrix} J_{p-2} & & & \\ & J_{q-p-1} & & 1 \\ & & \tilde{J}_{q-1} & -1 \\ & 1 & -1 & 0 \end{vmatrix}$$

$$\begin{aligned} &= (-1)^q(-1)^{q-1} \det J_{p-2} \cdot \det J'_{q-p-1} \cdot \det \tilde{J}_{q-1} \\ &\quad + (-1)^q(-1)^{q-2} \det J_{p-2} \cdot \det J_{q-p-1} \cdot \det \tilde{J}''_{q-1} \\ &= (-1)^q q(p-1)(q-p-1) + (-1)^{q-1}(q-1)(p-1)(q-p) \\ &= (-1)^{q-1} p(p-1). \end{aligned}$$

We have the following determinants which follow by induction,

$$\overline{J_n} = \begin{vmatrix} & J''_n \\ 1 & \end{vmatrix} = (-1)^2 \overline{J_{n-1}} = 1$$

and

$$\begin{vmatrix} & J_n \\ 1 & \end{vmatrix} = 0$$

Therefore,

$$
\begin{aligned}
\mathrm{cofac}_{12} = (-1)^{p-1} &\begin{vmatrix} J'_{p-2} & & & \\ & J_{q-p-1} & & 1 \\ & & \tilde{J}_{q-1} & -1 \end{vmatrix} \\
+ (-1)^{p} &\begin{vmatrix} J_{p-2} & & & \\ & J''_{q-p-1} & & 1 \\ & & \tilde{J}_{q-1} & -1 \end{vmatrix} \\
&= 0 + (-1)^{p}(-1)^{p-1}(-1)^{q-1}q(p-1) \\
&= (-1)^{q}q(p-1).
\end{aligned}
$$

$$\text{cofac}_{22} = \begin{vmatrix} J_{p-2} & & & 1 \\ & J_{q-p-1} & & 1 \\ & & \tilde{J}_{q-1} & \\ 1 & 1 & & 2 \end{vmatrix}$$

$$\begin{aligned} &= (-1)^{p-1}(-1)^{p} \det J'_{p-2} \cdot \det J_{q-p-1} \cdot \det \tilde{J}_{q-1} \\ &\quad + (-1)^{p}(-1)^{p-1} \det J_{p-2} \cdot \det J''_{q-p-1} \cdot \det \tilde{J}_{q-1} \\ &\quad + 2 \det J_{p-2} \cdot \det J_{q-p-1} \cdot \det \tilde{J}_{q-1} \\ &= (-1)^{q-1} q(q-1). \end{aligned}$$

As a result, we conclude that

$$\begin{aligned} c^2(W) &= (-2u, -2v) \begin{pmatrix} p(p-1) & q(p-1) \\ q(p-1) & q(q-1) \end{pmatrix} (-2u, -2v)^T \\ &= 4u^2 p(p-1) + 8uvq(p-1) + 4v^2 q(q-1). \end{aligned}$$

For the second example, recall that in the splicing of (I)-(I)-(I), we have the following intersection matrix:

$$Q = \left(\begin{array}{c|c|c|c|c} J_{p-2} & & & & 1 \\ \hline & J_{q-p-1} & & & \begin{matrix}1\\ & 1\end{matrix} \\ \hline & & J_{r-q-1} & & \begin{matrix}1\\ & 1\end{matrix} \\ \hline & & & \tilde{J}_{r-1} & \begin{matrix} & -1\\ & \end{matrix} \\ \hline \begin{matrix} & 1\\ & \end{matrix} & \begin{matrix}1\\ & \end{matrix} & \begin{matrix} & \\ 1 & \end{matrix} & \begin{matrix}1\\ & \end{matrix} & \begin{matrix}2 & \\ & 2\\ & \end{matrix} \\ & & \begin{matrix} & \\ & 1\end{matrix} & \begin{matrix}-1\\ & \end{matrix} & \begin{matrix} & \\ & 0\end{matrix} \end{array}\right)$$

Calculating determinant with respect to the last three rows as in the previous example, we have

$$\begin{aligned} \det Q &= (-1)^{r-1} r(r-q-1)(q-2) + (-1)^{r-1} r(r-q-2)(q-1) \\ &\quad - 2(-1)^{r-1} r(r-q-1)(q-1) \\ &\quad + (-1)^{r} (r-1)(r-q)(q-2) + (-1)^{r} (r-1)(r-q-1)(q-1) \\ &\quad - 2(-1)^{r} (r-1)(r-q)(q-1) \\ &= (-1)^{r-1}. \end{aligned}$$

Moreover, as we see in the given example, $c(W)$ evaluates on the given basis of $H_2(W;\mathbb{Z})$ as $w = (0, \ldots, -2u, -2v, -2y)^T$. In order to calculate c^2, it is sufficient to calculate

the inverse of the last 3×3 block of Q. Let us call this matrix D. We have

$$D = \begin{pmatrix} p(p-1) & q(p-1) & r(p-1) \\ q(p-1) & q(q-1) & r(q-1) \\ r(p-1) & r(q-1) & r(r-1) \end{pmatrix}.$$

We see that

$$\text{cofac}_{11} = \left|\begin{array}{ccccc} J_{p-2} & & & & \\ \hline & J_{q-p-1} & & & 1 \\ \hline & & J_{r-q-1} & & \begin{matrix} 1 & \\ & 1 \end{matrix} \\ \hline & & & \tilde{J}_{r-1} & \begin{matrix} -1 & \\ & 0 \end{matrix} \\ \hline & 1 & \begin{matrix} 1 & \\ & 1 \end{matrix} & \begin{matrix} & \\ -1 & \end{matrix} & \begin{matrix} 2 & \\ & 0 \end{matrix} \end{array}\right|$$

which can be calculated with respect to the last two rows so that

$$\begin{aligned}
\mathrm{cofac}_{11} &= \det J_{p-2} \cdot \det J'_{q-p-1} \cdot \det J'_{r-q-1} \cdot \det \tilde{J}_{r-1} \\
&\quad + \det J_{p-2} \cdot \det J_{q-p-1} \cdot \det J'''_{r-q-1} \cdot \det \tilde{J}_{r-1} \\
&\quad - 2 \det J_{p-2} \cdot \det J_{q-p-1} \cdot \det J'_{r-q-1} \cdot \det \tilde{J}_{r-1} \\
&\quad + \det J_{p-2} \cdot \det J'_{q-p-1} \cdot \det J_{r-q-1} \cdot \det \tilde{J}''_{r-1} \\
&\quad + \det J_{p-2} \cdot \det J_{q-p-1} \cdot \det J''_{r-q-1} \cdot \det \tilde{J}''_{r-1} \\
&\quad - 2 \det J_{p-2} \cdot \det J_{q-p-1} \cdot \det J_{r-q-1} \cdot \det \tilde{J}''_{r-1} \\
&= (-1)^{r-1} r(p-1)(p-r+1) + (-1)^r (r-1)(p-q)(p-r) \\
&= (-1)^{r-1} p(p-1).
\end{aligned}$$

Meanwhile,

$$\mathrm{cofac}_{22} = \begin{vmatrix}
J_{p-2} & & & & 1 \\
& J_{q-p-1} & & & 1 \\
& & J_{r-q-1} & & 1 \\
& & & \tilde{J}_{r-1} & -1 \\
1 & 1 & & & 2 \\
& & 1 & -1 & 0
\end{vmatrix}$$

which can be calculated with respect to the last two rows so that

$$\begin{aligned}
\operatorname{cofac}_{22} &= \det J'_{p-2} \cdot \det J_{q-p-1} \cdot \det J'_{r-q-1} \cdot \det \tilde{J}_{r-1} \\
&\quad + \det J_{p-2} \cdot \det J''_{q-p-1} \cdot \det J'_{r-q-1} \cdot \det \tilde{J}_{r-1} \\
&\quad - 2 \det J_{p-2} \cdot \det J_{q-p-1} \cdot \det J'_{r-q-1} \cdot \det \tilde{J}_{r-1} \\
&\quad + \det J'_{p-2} \cdot \det J_{q-p-1} \cdot \det J_{r-q-1} \cdot \det \tilde{J}''_{r-1} \\
&\quad + \det J_{p-2} \cdot \det J''_{q-p-1} \cdot \det J_{r-q-1} \cdot \det \tilde{J}''_{r-1} \\
&\quad - 2 \det J_{p-2} \cdot \det J_{q-p-1} \cdot \det J_{r-q-1} \cdot \det \tilde{J}''_{r-1} \\
&= (-1)^r q((p-2)(q-p) + (p-1)(q-p-1) - 2(p-1)(q-p)) \\
&= (-1)^{r-1} q(q-1).
\end{aligned}$$

Concurrently,

$$\operatorname{cofac}_{33} = \begin{vmatrix}
J_{p-2} & & & & 1 \\
\hline
 & J_{q-p-1} & & & \begin{matrix}1 \\ & 1\end{matrix} \\
\hline
 & & J_{r-q-1} & & 1 \\
\hline
 & & & \tilde{J}_{r-1} & \\
\hline
1 & \begin{matrix}1 \\ & 1\end{matrix} & 1 & & \begin{matrix}2 \\ & 2\end{matrix}
\end{vmatrix}$$

which can be calculated with respect to the last two rows so that

$$\begin{aligned}
\operatorname{cofac}_{33} &= \det J'_{p-2} \cdot \det J'_{q-p-1} \cdot \det J_{r-q-1} \cdot \det \tilde{J}_{r-1} \\
&\quad + \det J_{p-2} \cdot \det J'''_{q-p-1} \cdot \det J_{r-q-1} \cdot \det \tilde{J}_{r-1} \\
&\quad - 2 \det J_{p-2} \cdot \det J'_{q-p-1} \cdot \det J_{r-q-1} \cdot \det \tilde{J}_{r-1} \\
&\quad + \det J'_{p-2} \cdot \det J_{q-p-1} \cdot \det J''_{r-q-1} \cdot \det \tilde{J}_{r-1} \\
&\quad + \det J_{p-2} \cdot \det J''_{q-p-1} \cdot \det J''_{r-q-1} \cdot \det \tilde{J}_{r-1} \\
&\quad - 2 \det J_{p-2} \cdot \det J_{q-p-1} \cdot \det J''_{r-q-1} \cdot \det \tilde{J}_{r-1} \\
&\quad + 2 \det J'_{p-2} \cdot \det J_{q-p-1} \cdot \det J_{r-q-1} \cdot \det \tilde{J}_{r-1} \\
&\quad + 2 \det J_{p-2} \cdot \det J''_{q-p-1} \cdot \det J_{r-q-1} \cdot \det \tilde{J}_{r-1} \\
&\quad + 4 \det J_{p-2} \cdot \det J_{q-p-1} \cdot \det J_{r-q-1} \cdot \det \tilde{J}_{r-1} \\
&= (-1)^{r-1} r(r-1).
\end{aligned}$$

Note also that,

$$\overline{J_m} = \begin{vmatrix} 1 & \\ & J'_m \end{vmatrix} = (-1)^{m-1},$$

which follows by induction.

Therefore,

$$\text{cofac}_{12} = (-1)^{r-1}(-1)^{q-1}$$

$$\begin{array}{|c|c|c|c|c|}
\hline
J_{p-2} & & & & 1 \\
\hline
 & J'_{q-p-1} & & & 1 \\
\hline
 & & J'_{r-q-1} & & 1 \\
\hline
 & & & \tilde{J}_{r-1} & -1 \\
\hline
\end{array}$$

$$+ (-1)^{r-1}(-1)^{q}$$

$$\begin{array}{|c|c|c|c|c|}
\hline
J_{p-2} & & & & 1 \\
\hline
 & J_{q-p-1} & & & 1 \\
\hline
 & & J'''_{r-q-1} & & 1 \\
\hline
 & & & \tilde{J}_{r-1} & -1 \\
\hline
\end{array}$$

$$
+(-1)^{r-1}(-1)^{q-1}
\begin{vmatrix}
J_{p-2} & & & & 1 \\
& J'_{q-p-1} & & & 1 \\
& & J_{r-q-1} & & 1 \\
& & & \tilde{J}''_{r-1} & -1
\end{vmatrix}
$$

$$
+(-1)^{r-1}(-1)^{q}
\begin{vmatrix}
J_{p-2} & & & & 1 \\
& J_{q-p-1} & & & 1 \\
& & J''_{q-r-1} & & 1 \\
& & & \tilde{J}''_{r-1} & -1
\end{vmatrix}
$$

$$
= (-1)^{r-1}r(p-1)(r-q-1) + 0 + (-1)^{r}(r-1)(p-1)(r-q) + 0
$$

$$
= -(-1)^{r-1}q(p-1).
$$

Therewithal,

$$\operatorname{cofac}_{13} = \begin{vmatrix} J_{p-2} & & & & 1 \\ & J_{q-p-1} & & & 1 \\ & & & & 1 \\ & & J_{r-q-1} & & 1 \\ & & & \tilde{J}_{r-1} & \\ 1 & 1 & & & 2 \\ & & 1 & -1 & 2 \end{vmatrix}$$

which can be calculated with respect to the last two rows so that

$$\begin{aligned}
\operatorname{cofac}_{13} &= -(-1)^{r-1}(-1)^{p-1} \det J_{p-2} \cdot \det \overline{J'_{q-p-1}} \cdot \det \overline{J'_{r-q-1}} \cdot \det \tilde{J}_{r-1} \\
&\quad + (-1)^{r-1}(-1)^{p-1} \det J_{p-2} \cdot \det \overline{J_{q-p-1}} \cdot \det \overline{J'''_{r-q-1}} \cdot \det \tilde{J}_{r-1} \\
&\quad - (-1)^{r-1}(-1)^{q} 2 \det J_{p-2} \cdot \det J_{q-p-1} \cdot \det \overline{J'_{r-q-1}} \cdot \det \tilde{J}_{r-1} \\
&\quad - (-1)^{r-1}(-1)^{p-1} \det J_{p-2} \cdot \det \overline{J'_{q-p-1}} \cdot \det \overline{J_{r-q-1}} \cdot \det \tilde{J}''_{r-1} \\
&\quad + (-1)^{r-1}(-1)^{p-1} \det J_{p-2} \cdot \det \overline{J_{q-p-1}} \cdot \det J''_{r-q-1} \cdot \det \tilde{J}''_{r-1} \\
&\quad - (-1)^{r-1}(-1)^{q} 2 \det J_{p-2} \cdot \det J_{q-p-1} \cdot \det \overline{J_{r-q-1}} \cdot \det \tilde{J}''_{r-1} \\
&\quad + 2(-1)^{q-1}(-1)^{p-1} \det J_{p-2} \cdot \det \overline{J'_{q-p-1}} \cdot \det J_{r-q-1} \cdot \det \tilde{J}_{r-1} \\
&\quad + 2(-1)^{q}(-1)^{p-1} \det J_{p-2} \cdot \det \overline{J_{q-p-1}} \cdot \det J''_{r-q-1} \cdot \det \tilde{J}_{r-1} \\
&\quad + 4 \det J_{p-2} \cdot \det J_{q-p-1} \cdot \det J_{r-q-1} \cdot \det \tilde{J}_{r-1} \\
&= (-1)^{r-1} r(p-1).
\end{aligned}$$

Besides,

$$\text{cofac}_{23} = \begin{vmatrix} J_{p-2} & & & & 1 \\ & J_{q-p-1} & & & \begin{matrix}1\\ & 1\end{matrix} \\ & & J_{r-q-1} & & 1 \\ & & & \tilde{J}_{r-1} & \\ 1 & 1 & & & 2 \\ & & 1 & -1 & 0 \end{vmatrix}$$

which can be calculated with respect to the last two rows so that

$$\begin{aligned}
\text{cofac}_{23} &= (-1)^{r-1}(-1)^{q-1} \det J'_{p-2} \cdot \det J_{q-p-1} \cdot \det \overline{J'_{r-q-1}} \cdot \det \tilde{J}_{r-1} \\
&\quad + (-1)^{r-1}(-1)^{q-1} \det J_{p-2} \cdot \det J''_{q-p-1} \cdot \det \overline{J'_{r-q-1}} \cdot \det \tilde{J}_{r-1} \\
&\quad - (-1)^{r-1}(-1)^{q-1} 2 \det J_{p-2} \cdot \det J_{q-p-1} \cdot \det \overline{J'_{r-q-1}} \cdot \det \tilde{J}_{r-1} \\
&\quad + (-1)^{r-1}(-1)^{q-1} \det J'_{p-2} \cdot \det J_{q-p-1} \cdot \det \overline{J_{r-q-1}} \cdot \det \tilde{J}''_{r-1} \\
&\quad + (-1)^{r-1}(-1)^{q-1} \det J_{p-2} \cdot \det J''_{q-p-1} \cdot \det \overline{J_{r-q-1}} \cdot \det \tilde{J}''_{r-1} \\
&\quad - (-1)^{r-1}(-1)^{q-1} 2 \det J_{p-2} \cdot \det J_{q-p-1} \cdot \det \overline{J_{r-q-1}} \cdot \det \tilde{J}''_{r-1} \\
&= -(-1)^{r-1} r(q-1).
\end{aligned}$$

As a result, we conclude that

$$c^2(W) = (-2u, -2v, -2y) \begin{pmatrix} p(p-1) & q(p-1) & r(p-1) \\ q(p-1) & q(q-1) & r(q-1) \\ r(p-1) & r(q-1) & r(r-1) \end{pmatrix} (-2u, -2v, -2y)^T$$

$$= 4u^2p(p-1) + 4v^2q(q-1) + 4y^2r(r-1)$$

$$+ 8uvq(p-1) + 8uyr(p-1) + 8vyr(q-1).$$